Review

CONTRAST MEDIA & MOLECULAR IMAGING

Received: 13 May 2014, Accepted: 18 September 2014, Published online in Wiley Online Library

(wileyonlinelibrary.com) DOI: 10.1002/cmmi.1630

Electron paramagnetic resonance: a powerful tool to support magnetic resonance imaging research

Pierre Danhier and Bernard Gallez*

The purpose of this paper is to describe some of the areas where electron paramagnetic resonance (EPR) has provided unique information to MRI developments. The field of application mainly encompasses the EPR characterization of MRI paramagnetic contrast agents (gadolinium and manganese chelates, nitroxides) and superparamagnetic agents (iron oxide particles). The combined use of MRI and EPR has also been used to qualify or disqualify sources of contrast in MRI. Illustrative examples are presented with attempts to qualify oxygen sensitive contrast (i.e. T_1- and T_2*-based methods), redox status or melanin content in tissues. Other areas are likely to benefit from the combined EPR/MRI approach, namely cell tracking studies. Finally, the combination of EPR and MRI studies on the same models provides invaluable data regarding tissue oxygenation, hemodynamics and energetics. Our description will be illustrative rather than exhaustive to give to the readers a flavour of 'what EPR can do for MRI'. Copyright © 2014 John Wiley & Sons, Ltd.

Keywords: EPR; MRI; contrast agent; nitroxide; oxygen; iron oxide

1. INTRODUCTION: NMR VERSUS EPR

Historically, electron paramagnetic resonance (EPR) [or equivalently electron spin resonance (ESR)] and nuclear magnetic resonance (NMR) were discovered at the same period of time. In 1944, Zavoisky first described the EPR phenomenon (1,2). A little later, Bloch and Purcell discovered the NMR phenomenon (3,4). In 1973, Lauterbur published the original idea of applying magnetic field gradients in three dimensions to create NMR images (5). Since that time, MRI has been extensively developed and has revolutionized medical imaging. In other respects, the first *in vivo* EPR experiments were carried out in 1975 (6,7) and the first EPR imaging (EPRI) experiment was reported in 1979 (8,9). In comparison with the flourishing applications of MRI for the diagnosis and treatment of human diseases, the development of *in vivo* EPR and EPR imaging has been rather slow. There are several reasons for this, especially linked to the considerable technical challenges that make *in vivo* EPR difficult (7,10).

There are few fundamental differences between the principles of electron and nuclear magnetic resonance as NMR- and EPR-related techniques share similar basic principles. However, the differences in physical and chemical properties of the resonant species (unpaired electrons vs nuclei with net spin) lead to profound differences in the techniques that are used to record the spectra or to reconstruct an image (7,10–12) (Table 1). There are three major differences between EPR and NMR: (a) the size of the magnetic moments, which fixes the ratio between the frequency and the magnetic field; (b) the very short relaxations times of the electron spins compared with the nuclear spins; and (c) the limited amounts of paramagnetic materials that are present in most biological systems.

The gyromagnetic ratio of an unpaired electron is much larger than that of a proton, so the resonance frequency/magnetic field ratio for the electron is 28 GHz/T vs 42.5 MHz/T for the proton. As a consequence, standard EPR spectrometers operate at much higher frequencies (microwaves) and lower fields than NMR spectrometers: the most usual commercial EPR spectrometers operate at 9 GHz (X-band) for a magnetic field around 0.34 T. At this high frequency, the nonresonant absorption of the electromagnetic radiation by the liquid water presents serious problems, and limits the sample size to 1 mm. Classical *in vitro* EPR experiments on cells are carried out in thin capillary tubes, and *in vivo* experiments at 9 GHz are limited to pharmacokinetic studies on the tail vein of mice (13,14). Larger aqueous samples or animals can be studied only by reducing the operating frequency, for example by using 1 GHz spectrometers (L-band) (15–17). At 1 GHz, the depth of penetration is of about 1 cm, but with a reduced sensitivity.

A second major difference between NMR and EPR is related to the relaxation times. While longitudinal T_1 and transversal T_2 relaxation times of protons are in the range of 0.1–1 s (18), electronic spins return to the equilibrium after excitation much more rapidly (ns to μs). This feature has two consequences. First, EPR spectra in biological systems are mostly obtained through continuous wave experiments. Instead of applying an energy pulse and recording the transient response as done in NMR and MRI, the sample is continuously irradiated with a low-power microwave radiation while the magnetic field is gradually increased so that electron spins come into resonance. So far, only a few groups have succeeded in addressing the challenges of time-

* *Correspondence to: Bernard Gallez, Biomedical Magnetic Resonance Research Group, Louvain Drug Research Institute, Université catholique de Louvain, Avenue Mounier 73.08, B-1200 Brussels, Belgium. E-mail: bernard.gallez@uclouvain.be*

P. Danhier, B. Gallez
Biomedical Magnetic Resonance Research Group, Louvain Drug Research Institute, Université catholique de Louvain, Brussels, Belgium

Biographies

Pierre Danhier is born in 1986 in Brussels in Belgium. He graduated with a PhD in Pharmaceutical Sciences from the Université catholique de Louvain (Belgium) in 2013. The PhD was completed in the biomedical resonance unit group from Professor Bernard Gallez. Research led during the PhD focused on tracking *in vivo* metastatic cancer cells using magnetic resonance approaches. He is currently occupying a postdoc position under the supervision of Professor Zaver Bhujwalla at the Johns Hopkins University (Baltimore, USA), studying the link between tumor hypoxia and metastasis using optical imaging.

Bernard Gallez is born in 1964 in Mons (Belgium). He is pharmacist (1988), industry pharmacist and radiopharmacist (1990), and got his PhD in 1993 with a work focused on the targeting of MRI contrast agents. He made a post-doc in Dartmouth where he learned in vivo EPR. In Brussels, he built the Biomedical Magnetic Resonance laboratory with a focus on the development of new MR technologies (MRI and EPR) and their applications to the characterization and manipulation of the tumor microenvironment and the hemodynamic process in tissues (oxygenation, perfusion, oxygen consumption, angiogenesis).

Table 1. Comparison between NMR and EPR

	EPR	NMR
Detectable species	Compounds with unpaired electron(s)	Compounds with nuclear spin $I \neq 0$
Frequency/magnetic Field ratio	28 GHz/T	42.5 MHz/T
Relaxation time	ns–μs	ms–s
Need for exogenous probes	• *No* for stable paramagnetic species (Mn, iron oxides, etc.) • *Yes* for labile radicals (spin trapping) • *Yes* for oximetry (spin labeling)	*No* (H_2O concentration in living organisms >50 M)
Sensitivity	• High *in vitro* or *ex vivo* (<nM) • Limited *in vivo* owing to RF absorption by water	• Low (~10^{-4} M) • Improved thanks to contrast agents (Gd, iron oxides, etc.) for imaging applications
Clinical applications	Limited so far: oximetry (spectroscopy) and retrospective dosimetry	Wide range of imaging applications owing to: • a high anatomical and temporal resolution • variety of source of contrasts

domain EPR *in vivo* (19–21). The second consequence of short EPR relaxation times is that EPR imaging requires the application of magnetic gradients that are much larger than those used in MRI (11).

The third but not the least difference between both MR techniques relies on the nature of the material that is studied. Compared with the 100 M concentration of endogenous protons available for NMR, there is a lack of sufficient amounts of naturally occurring paramagnetic materials for EPR. Except for melanin that can be easily detected in biological samples (22–26), endogenous paramagnetic species are present in insufficient amounts to be detected by *in vivo* EPR. The short half-life of most free radicals involved in physiology (such as nitric oxide) or in toxicology (such as superoxide or hydroxyl radicals) is another source of difficulty. These reactive species are usually detected using a spin-trapping strategy by the formation of a stable spin adduct after reaction with a nitrone (27). Generally, for *in vivo* and *in vitro* EPR biological studies, a stable paramagnetic material has to be introduced in the biological system to be detected. Very interestingly, the paramagnetic reporter may provide unique information on its environment such as *in vitro* and *in vivo* oxygenation (28–32), redox status (33,34), pH (35–38) or microviscosity (39,40).

For those not familiar with EPR spectroscopy, it should be acknowledged that the main parameters derived from EPR spectra are the *g-values* (analogous to the chemical shift in NMR), the electron–nuclear hyperfine coupling constants (analogous to nuclear spin–spin coupling constants in NMR), linewidths and intensities (41). Because EPR spectra are usually displayed as first derivatives, linewidths are conveniently measured as the distance between points of maximum and minimum slope. Intensities are often measured as the amplitude of each line, but it is preferable to use the double integration of the signal to assess the concentration in a paramagnetic species.

While the development of *in vivo* EPR is a research field *per se*, there is an outstanding potential of EPR-related methods to support MRI developments. The purpose of this manuscript is to describe some of the areas where EPR has provided unique information to MRI developments. The field of application mainly encompasses the EPR characterization of MRI paramagnetic

contrast agents (gadolinium and manganese chelates, nitroxides) and superparamagnetic agents (iron oxide particles). The combined use of MRI and EPR has also been used to qualify or disqualify sources of contrast in MRI. Illustrative examples are presented with attempts to qualify oxygen sensitive contrast (i.e. T_1- and T_2*-based methods), redox status or melanin content in tissues. Other areas are likely to benefit from the combined EPR/MRI approach, namely cell tracking studies. Finally, the combination of EPR and MRI studies on the same models provide invaluable data regarding tissue oxygenation, hemodynamics and energetics. Our description will be illustrative rather than exhaustive to give to the readers a flavour of 'what EPR can do for MRI'. A comprehensive review on this research field was published about 10 years ago (42), so an update is timely.

2. CHARACTERIZATION OF MRI CONTRAST AGENTS PROPERTIES WITH EPR

Despite its richness in sources of contrast and its high spatial resolution, MRI lacks sensitivity. It is generally admitted that the use of contrast agents (CAs) may counterbalance this default. Seeking innovative tissue-selective and smart CAs is a major research area for many academic groups and pharmaceutical companies. Virtually all MRI contrast agents contain species with unpaired electrons so that EPR is a method of choice for direct study of their properties. The interaction between the electron magnetic moment and the nuclear spin moment of the water proton will induce an increase in the proton relaxation rates. The relaxivity defines the ability of a CA to affect the relaxation rate of the surrounding protons. The effect of a CA on the MR image will mainly depend on the r_2/r_1 ratio, where r_1 is the longitudinal relaxivity and r_2 is the transversal relaxivity ($s^{-1}\,mM^{-1}$). On the one hand, paramagnetic CAs such as lanthanide derivatives exhibit a low r_2/r_1 ratio (typically, between 1 and 2) and will enhance the signal on T_1-weighted images when present at low concentration. Such contrast agents are thus called positive CAs. On the other hand, superparamagnetic and ferromagnetic CAs such as iron oxide particles exhibit a high r_2/r_1 ratio (as high as 50) and will decrease the signal on T_2-weighted images. Such contrast agents are called negative CAs. As described hereafter, EPR may provide invaluable information on both classes (paramagnetic and superparamagnetic) of CAs.

2.1. Exogenous Paramagnetic Contrast Agents

2.1.1. Gadolinium

Gadolinum complexes represent the major class of positive CAs used in the clinic. The use of chelating agents is required to prevent toxicity of gadolinium and ensure an effective elimination of the metal. The first generation of gadolinium-based CAs encompasses highly hydrophilic low-molecular-weight complexes with an extracellular biodistribution (based on the DTPA or the DOTA structure). Later on were developed compounds bearing more lipophilic chains in order to modulate the biodistribution with a partial biliary elimination (Gd–EOB–DTPA or gadoxetate, and Gd–BOPTA or gadobenate) and long blood circulation through interactions with albumin (MS-325 or gadofosveset). When developing new Gd-based CAs, it is mandatory to fully characterize the kinetic and thermodynamic stability of the complex (43), the pharmacokinetic profile as well as the relaxivity of the new agent. The relaxivity of a CA can be described by taking into account the 'inner sphere' and the 'outer sphere' contributions (44). Briefly, the inner sphere contribution relies on the exchange of water molecules remaining in the primary coordination site and the bulk solvent whereas outer sphere relaxation mechanisms involve distant interactions between paramagnetic gadolinium and bulk water molecules. The inner sphere contribution is the most effective and governed by four correlation times: the rotational correlation time of the complex (τ_R), the residence time of a water proton in the inner coordination sphere (τ_m) and its chemical exchange with bulk water, and the electronic longitudinal and transverse relaxation rates ($1/T_{1e}$ and $1/T_{2e}$) of the metal center. The characterization of the contrast agents is generally obtained thanks to the measurements of relaxivities at different field strengths (NMRD profiles). To elucidate the different contributions to the observed relaxivity of soluble Gd-based CAs, NMRD profiles can advantageously be supplemented by a combination of ^{17}O studies that measure water exchange rates and EPR spectrometry studies that provide precise measurements of the electronic spin relaxation times (45–51). This simultaneous analysis of experimental data helps to solve the problem of the interdependence of parameters in NMRD analysis and yields to physically meaningful values (52,53). Although less attention has been devoted to the influence of electronic relaxation on the relaxivity, it was worthwhile to investigate how different ligand designs could optimize the electron spin relaxation properties. The overall transverse electronic relaxation rates, $1/T_{2e}$, can be obtained from the peak-to-peak EPR line widths of the derivative spectra, and the electron spin relaxation rates for Gd(III) complexes are usually interpreted in terms of a transient zero-field splitting (ZFS) mechanism induced by distortions of the complex (45). A series of more in-depth studies analyzed the contribution of the static ZFS and transient ZFS to the electronic relaxation (53–56). Indeed, the structure and the dynamics of the electronic density of the chelate framework that surrounds the metal determine the ZFS and therefore the electron spin relaxation rates in solution. This was achieved by recording EPR spectra at different temperatures and frequencies on different gadolinium complexes. Overall, these studies performed on many different Gd chelates demonstrate that, for fast rotating molecules, electronic relaxation has little influence on the efficiency of Gd(III)-based MRI contrast agents at high magnetic fields ($B > 3\,T$), but may have a marked influence at low magnetic field. In other words, the relatively long electronic relaxation time of Gd-based contrast agents (compared with other metals) is not the limiting factor in the relaxivity, at least at the field strengths presently used by the MRI clinical scanners.

The EPR studies were not limited to the study of soluble Gd-based CAs and were also applied for the characterization of nanoparticles. In a study on Gd(III)-doped zeolite NaY nanoparticles (57), EPR spectra suggest that an interaction between neighboring Gd^{3+} ions within the same particle produces a significant increase in the transversal electronic relaxation rates in samples with a high Gd^{3+} content. A recent study was carried out on gadolinium oxide or gadolinium hydroxyde nanoparticles as well as on dysprosium, holmium, terbium and erbium containing particles (58). For these latter compounds, the combination of NMR and EPR studies with theoretical simulations showed that T_2 relaxation is caused by water diffusion in the field inhomogeneities created by the magnetic particle. The different relaxation behaviors were caused by different electron

relaxation times, as estimated by EPR (58). Other EPR studies focused on the interactions of lipophilic Gd-based CAs with biological membranes (59). It was shown that the spin label EPR method using nitroxides can be used to detect the presence and possible location of lipophilic CAs in the model membranes, the changes and distortions in membrane organization, and the changes in the local polarity of the bilayer due to addition of Gd^{3+} complexes (59). This work also demonstrated that interaction of Gd^{3+} complexes with phospholipid bilayers can be observed directly from changes in their EPR spectra. In addition, the analysis of frequency dependence of the *g*-factors provided estimates of the ZFS parameter in physiological conditions and information on how this parameter was affected by interaction with lipids. In a recent study, Lagerstedt *et al.* used a combination of EPR and relaxivity studies to characterize Gd-labeled apoA-lipoprotein A-I as a MRI contrast agent (60). This protein contrast agent was obtained by attaching the thiol-reactive Gd label at Cys residues replaced at four distinct positions in apoA-I. The authors found out that that putative site-directed protein contrast agents can be screened by X-band EPR spectroscopy employing both nitroxide and Gd(III)–DOTA probes. According to the authors (60), the main advantage of using EPR spectroscopy is that the concentration of the protein is significantly lower (~10 μM spin for nitroxide-labeled and ~1 mM for Gd(III)-labeled sample) than is necessary in NMR spectroscopy (>100 μM protein). Moreover, the sample volume for EPR experiments (~5 μl) is about two orders of magnitude smaller than that used for NMR measurements (~500 μl).

Eventually, EPR was also used for the gadolinium quantification in tissues (61). Although the quantification of Gd in tissues is undeniably important when trying to target CAs to different receptors, surprisingly, EPR spectroscopy has been applied for this purpose only exceptionally. An example was the application of EPR to quantify Gd-labeled vesicles targeted to overexpressed glucose receptors in tumors (61). The quantification of the Gd signal intensity is a straightforward method and has the potential to be issued for many other applications. More recently, an alternative indirect method has been suggested by Takeshita *et al*. (62). They used a spin labeling approach by using nitroxide solutions. The presence of paramagnetic Gd induces a decrease in the T_{2e} and consequently an EPR linebroadening. They found a linear relationship between the concentration of Gd-CAs and the linewidth of the nitroxide probe. Possible applications encompass the Gd quantification in plasma (62).

2.1.2. Manganese

Manganese is a paramagnetic transition metal that possesses five free electrons. Mn^{2+} has a low r_2/r_1 ratio and serves as a positive CA on T_1-weighted images (63). In experimental studies, an interesting feature of Mn^{2+} is its ability to mimick Ca^{2+} *in vivo*. As calcium, manganese ions enter in cells via voltage-gated Ca^{2+} channels. Mn^{2+} can be taken up by neurons and move along axons to reach synapses (64,65). Hence, manganese-enhanced MRI (MEMRI) was increasingly developed to study the functional connectivity patterns in small animals (66,67). MEMRI is mostly performed using infusions of $MnCl_2$. Unfortunately, as Mn^{2+} is neurotoxic (68,69) through the accumulation in the striatum (70,71), it is unlikely that MEMRI applications will eventually be possible in humans. The use of chelates to prevent the toxicity of Mn^{2+} was investigated and one compound, Mn-DPDP (Mn-dipyridoxaldiphosphate or mangafodipir), was used in humans for hepatobiliary imaging (72). Rapidly, several reports suggested an *in vivo* dissociation of the Mn-chelate. These assumptions were actually based on the fact that the signal enhancement was persistent after injection in organs where free manganese is known to accumulate (44,73). EPR played a key role in the direct evidence for the dissociation (73). At 9 GHz, free Mn^{2+} provides a six-line-EPR spectrum whereas bound manganese is EPR silent (73,74). These features allowed the study of the dissociation of Mn-DPDP in biological tissues (73). Further evidence for this dissociation was provided by radiolabeling studies using different isotopes for the ligand and for the metal (75). Interestingly, these EPR and isotope studies were in agreement with the changes in ^{31}P-NMR spectra obtained in tissues (73,76). Further EPR studies at different frequencies confirmed the dissociation and suggested the role of Zn^{2+} in the transmetallation of Mn-DPDP (74). These EPR data were important to question the relaxation properties of Mn-DPDP. Indeed, it was found that the Mn^{2+} released by the complex was binding to proteins, this association being responsible for the large increase in the T_1 relaxivity (73,74). As a consequence of this set of evidence for the dissociation of the Mn complex, it was found that the transport into the hepatic cells was not mediated by the pyridoxine transporter (76,77). It also raised concerns about the possible accumulation of free manganese in the brain and possible associated toxicity (78–80). Although mangafodipir is no longer commercialized, research on Mn-based chelates is still active, and it is likely that EPR may contribute to the characterization of these potential CAs.

2.1.3. Nitroxides

Nitroxide compounds are stable organic molecules that possess one unpaired electron (Fig. 1). As gadolinium manganese-based compounds, nitroxides have been proposed as positive CAs for MRI (81–83). The development of nitroxides as MRI CAs was rather challenging because their relaxivity is unfavorable compared with metal-based agents. Contrary to Gd-based compounds, the main contribution is due to a distant interaction between the free electron and the water, and the contribution of the inner-sphere process for hydrophilic nitroxide is considered to be negligible. There were several attempts to increase the relaxivity of nitroxides, namely by using the immobilization of nitroxides directly linked to macromolecules (84–88) or strongly interacting with proteins such as albumin because of their large lipophilicity (89–93). EPR studies demonstrate that the degree of immobilization as evidenced by EPR spectrometry was directly correlated to an increased NMR r_1 relaxivity (86). In addition, it was shown that the number of lipophilic nitroxides adsorbed on albumin (as quantified by EPR spectroscopy) was directly responsible for the increased relaxivity (91).

One challenge that appeared when using nitroxides as MRI CAs is the rapid elimination of the compounds by a metabolic reaction. The paramagnetic nitroxide is rapidly reduced and converted into the corresponding diamagnetic hydroxylamine (Fig. 1), an effect that leads to the fading and disappearance of the contrast induced by the nitroxide on the MR image. Systematic EPR and/or MRI studies were carried out to establish the structure/reactivity relationships of the nitroxides (94–99). It also appeared that this bioreduction was dependent on the oxygenation and the redox status of the tissues (94,100–102). The group of H. M. Swartz understood the value of turning the problem of nitroxide metabolism into virtues, and developed the concept

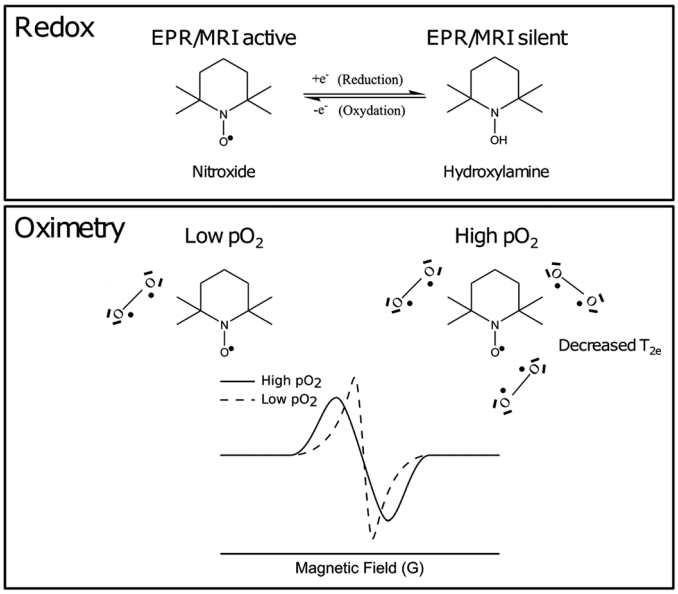

Figure 1. The versatile role of nitroxides (=nitroxyl radicals) for redox and oximetry studies. As shown in the upper panel, paramagnetic nitroxides can be reduced in biological media into electron paramagnetic resonance (EPR) silent hydroxylamines. The rate of decrease in the EPR signal intensity reflects thus the redox state of the surrounding environment. For oximetry studies (lower panel), electronic transversal relaxation times (T_{2e}) of nitroxides are affected by the presence of surrounding oxygen molecules. Therefore the linewidth of the EPR spectrum of a nitroxide is proportional to the pO_2 of the sample.

of functional contrast agents that are sensitive to the oxygenation and to the redox status. Historically, this is probably one of the first example of MRI 'smart contrast agents' that are activated or deactivated in the presence of a key factor present inside a tissue. The seminal ideas of using these compounds as redox-sensitive contrast agents are still being actively developed in EPR imaging (103–108) and in MRI (13,34,109–113). In these strategies to qualify these redox-sensitive CAs, we may say that EPR and MRI are complementary because EPR is monitoring directly the concentration of the nitroxide and indirect measurements with MRI provide images with a higher resolution. Moreover, MRI systems are more widespread and accessible to a larger imaging community. However, special care should be taken when linking the signal decay of the nitroxides to the redox status because the kinetics of clearance may also depend on the perfusion (and wash-out from the tissue) and on the viability of the cells (13). Again, direct measurements by EPR may resolve the origin of the decrease in nitroxide concentration (13).

Another possible interesting application is the ability to target nitroxides to specific tissues or receptors. Actually, the nitroxide moiety can be anchored to any specific organic entity that will be responsible for the biodistribution and the accumulation in a tissue of interest. Historically, small hydrophilic nitroxides were first used as positive MRI CAs (82,83,114,115). Later on, larger molecules bearing nitroxides were tested. In addition to the increase in relaxivity linked to the immobilization of the nitroxides, longer blood half-life and slower kidney elimination were obtained (87,116). The first example of targeting of nitroxides was the development of liver-specific CAs. This was achieved with the synthesis and evaluation of nitroxide fatty acid derivatives recognizing the Fatty Acid Binding Protein responsible for the internalization of these derivatives in the hepatocytes (90,91). Another target present at the surface of the hepatocytes was the asialoglycoprotein receptor. Polysaccharides bearing galactose residues, such as arabinogalactans, were functionalized with nitroxides (85). In each case, EPR, relaxometry and *in vivo* MRI studies were used in combination to characterize these MRI CAs. Other compounds were developed in order to gain in liver selectivity thanks to an accumulation in another compartment of the liver, the Kuppfer cells, for example using liposomes including lipophilic compounds (117). More recently, lipophilic compounds able to cross the blood–brain barrier were developed and evaluated as EPRI and MRI CAs (108,110,118–123). Finally, in a limited series of studies, EPR spectroscopy was also used to understand how pathological situations affecting liver function and kidney elimination was affecting the kinetics of elimination of nitroxide CAs (124).

2.2. Exogenous Superparamagnetic Contrast Agents

Superparamagnetic iron oxide particles (SPIO) CAs exhibit a high r_2/r_1 ratio and induce a signal loss on T_2- and T_2*-weighted images. The SPIOs may vary in size and in the coating surrounding the magnetic iron oxide core, properties that affect their stability and physico-chemical properties. The readers are invited to consult a comprehensive review of Laurent *et al.* to learn more on the chemical synthesis of these particles, the relationships between their physico-chemical design and their magnetic properties and how the constituents of the coating modulate the biological properties (125). The first generation of SPIOs that were developed accumulated preferentially in cells belonging to the reticulo-endothelial system (i.e. Kuppfer cells in liver) and was mainly used as liver CAs. Hence, clinically approved ferumoxides were designed for improving the detection of liver tumors (126–128). Ultrasmall iron oxide particles (USPIOs) with a diameter lower than 20 nm are less taken up by the liver and have a longer blood half-life. They may be used as blood pool agents (129,130) or lymphotropic agents (131–133). In the recent years, intense research has been devoted to attempts to functionalize the USPIOs with appropriate targeting molecules

in order to confer on them a high selectivity to tissues or molecular targets overexpressed in specific diseases (125,134–138). The modulation of the biodistribution of iron particles is theoretically more attractive than gadolinium. Indeed, iron oxides can be detected at lower concentration than gadolinium thanks to their higher relaxivities. Moreover, the degradation of the iron core over the time and the physiological iron recycling will preclude the accumulation of a toxic metal contrarily to gadolinium (139,140), although each functionalized iron oxide platform should be carefully checked for potential toxicity (141–145). Because iron oxide particles induce a decrease in the MR signal intensity on T_2- and T_2*-weighted images, the qualification of new CAs should carefully address the origin of the recorded induced hyposignal. Indeed, several physiological events or artifacts linked to the presence of air cavities, blood vessels, bone–tissue interfaces and hemorrhages may also be responsible of signal voids and may be confounding factors on T_2- and T_2*-weighted images (146,147). Generally, the accumulation of the iron oxides in the tissue of interest is confirmed by histochemistry using Prussian Blue staining (148), but this technique is qualitative and not quantitative. The assessment of the concentration of iron oxides particles in tissues of interest represents an important step in the qualification of new CAs (149). To achieve that goal, radioactive ^{59}Fe-SPIO can be used, but this requires the chemical synthesis of radiolabeled nanoparticles (139) which is cumbersome. Inductively coupled plasma mass spectrometry (ICP-MS) or inductively coupled plasma optical emission spectrometry (ICP-OES) are alternatives that provide a sensitive quantification of elemental iron in tissues (150–152). However, it should be noted that this method is unable to discriminate endogenous iron from exogenous iron oxide nanoparticles. In this respect, EPR spectroscopy is invaluable because the EPR spectrum exhibits different lines for the different chemical forms of iron. The iron oxide contained in SPIOs exhibit a broad and intense EPR spectrum whereas that can be easily differentiated from the free Fe^{3+} ion (153,154) (Fig. 2). A comparison study demonstrated that *ex vivo* EPR spectroscopy was superior to ICP-OES for assessing the SPIO biodistribution after administration (155). Historically, the first application of EPR for quantification of iron oxides in tissues was done on the liver of mice that received SPIOs administration in a model of septic shock (156). As new (U)SPIO particles are currently extensively designed for molecular imaging, theranostic, that is, combining diagnosis and treatment using the same platform, *ex vivo* EPR spectroscopy appears to be a reliable tool to monitor iron oxide nanoparticles after injection. Recent applications in this area demonstrated the usefulness of EPR to determine the concentration of USPIOs targeted to E-selectin in the context of the MRI detection of inflammation (154). By combining EPR and MRI, it was demonstrated that these USPIOs covered with a hexapeptide could be a useful molecular MRI marker for the noninvasive diagnosis and monitoring of inflammation (154). Interestingly, it was even possible to use low-frequency EPR to monitor directly *in vivo* the accumulation of these USPIOs in inflamed tissues. These EPR and MRI data supported the interest for the active targeting by grafting the particles with these peptides compared with ungrafted particles. More recent studies used a similar approach to qualify USPIOs targeting dying cells (157,158). USPIOs covered with hexapeptides targeting the phosphatidylserine were shown to induce a signal loss in apoptotic areas within tumors on T_2-w images. The same particles were shown to constitute an earlier MR biomarker of tumor cell death (after cytotoxic treatments) compared with diffusion-weighted-MRI and choline measurement by ^{1}H MRS. EPR spectroscopy was used in these studies to validate the MR data (157,158). It is likely that this application of EPR may be extended to many iron oxides particles platforms in the search

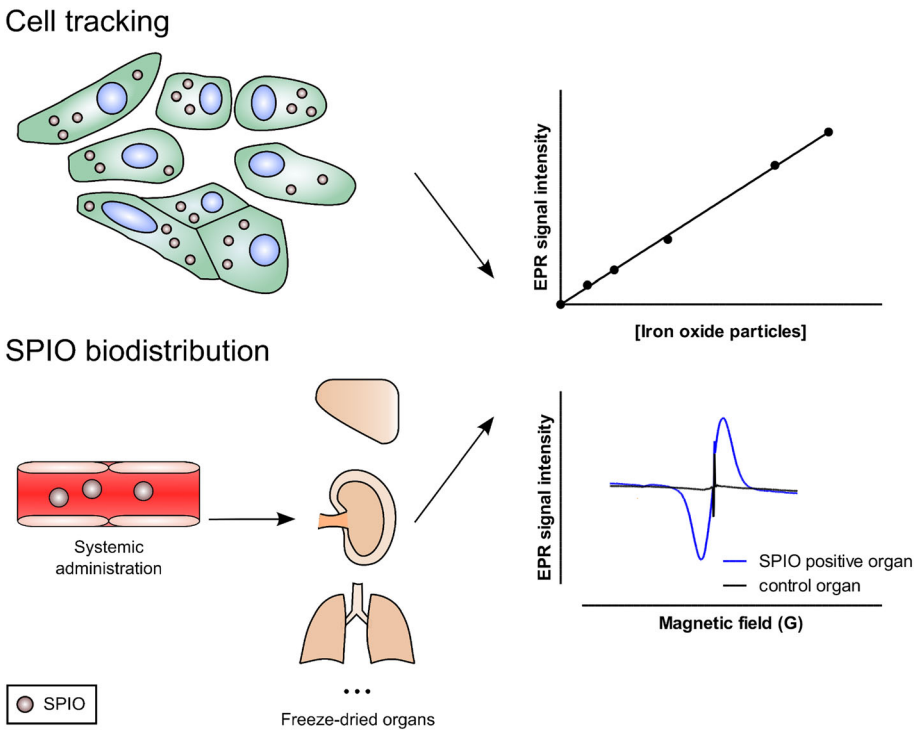

Figure 2. EPR as a sensitive tool to assess the iron oxide content in cells and tissues. Iron oxides (e.g. superparamagnetic iron oxide particles, SPIO) exhibit a typical EPR spectrum whereas endogenous iron in biological samples does not. There is a linear relationship between the iron oxide concentration and the EPR signal intensity. Iron oxides concentrations can be measured using EPR in isolated cells or freeze-dried organs.

of new CAs. Although EPR has mostly been used for iron oxide quantification, EPR was also used in one study in combination with magnetometry and relaxometry to elucidate the mechanism of T_2-shortening induced by monocrystalline iron oxide particles (159).

3. MELANIN AS AN ENDOGENOUS MRI CONTRAST AGENT?

Melanin is a paramagnetic polymeric molecule produced by melanocytes to prevent the toxicity of ultraviolet radiations (160). Eumelanin is also produced by pigmented melanoma, a skin cancer that is responsible for 75% of the deaths linked to skin cancer (161). When the malignant melanoma is small and well localized, removal of the tumor with surgery is often sufficient to cure the patient. If the lesion has spread to distant deep tissues, the 5-year survival drops below 10% (162). This poor outcome for advanced diseases highlights the need for early diagnosis modalities. Visual inspection, dermoscopy and biopsies are the most used methods to stage malignant melanoma (163,164). Owing to the paramagnetic properties of melanin, MRI and EPR imaging may potentially be valuable to visualize human skin melanomas and metastases (22–26,165). Most EPR studies conducted so far have been carried out *ex vivo*, but the first image of this endogenous radical has been achieved at low frequency on mice bearing the B16 melanoma model (22). Melanoma metastases are often found in the brain and have been suggested to have a specific MR signature based on their relaxation times (166). However, this specific contrast pattern is subject to widespread debate and several studies have reported disparate results (167,168). In addition to the melanin content, it should be noticed that the MR contrast of melanoma lesions can also be influenced by the presence of metallic ions and the presence of hemorrhages that are often associated with cancer lesions (169,170). Although a correlation was found between the melanin presence in human biopsies (revealed by histopathology analysis) and T_1 values (166,168), only *in vitro* experiments have shown a correlation between the melanin content and T_2 values (171). As the content in paramagnetic melanin can be accurately quantified by EPR, this method was recently used to try to elucidate the possible role of melanin in the MRI contrast (172). This study compared systematically the content in paramagnetic melanin in the tumors and the T_1, T_2 and T_2* contrast at high field. This was achieved on different models of melanoma presenting different pigmentation. It was actually found that the melanin alone has a negligible effect on the MRI contrast (172) and that other sources like the binding of melanin to metals are likely to have a key role, hence providing a unique response to this historical debate.

4. EPR/MRI APPLICATIONS IN CELL TRACKING

Cell tracking can be defined as the noninvasive monitoring of individual cells after injection *in vivo* using imaging techniques. This approach allows the assessment of the biodistribution of cells and their survival after implantation (173). Cell-based therapies (173) and cancer research (174–176) are the main fields of application of cell tracking. The label can be a reporter gene, for example, the luciferase gene for optical imaging (177), or a contrast agent that is incorporated within the cytoplasm of the cell (147). MRI is a suitable modality to perform cell tracking owing to its high anatomical resolution. Gadolinium agents can in principle be used for cell tracking, but their low relaxivity compared with iron oxide particles leads to the use of large concentrations of intracellular gadolinium to be detected (~10^{-4} to 10^{-5} M) (147). Therefore, iron oxide particles such as SPIO or microparticles of iron oxide (MPIO, with a diameter of about 1 μm) are largely preferred because these particles induce a strong contrast on T_2- and T_2*-weighted images so that single cell tracking is feasible (176,178–182). Intracellular incorporation of a sufficient amount of CAs is an important preliminary step to perform efficient cell tracking. Quantification of internalized iron oxide particles is thus mandatory to optimize labeling strategies. To reach that goal, the same methods than those described for assessing the content of iron oxides in tissues may be used (149). In this context, EPR was shown to be a sensitive, specific and a reliable method to quantify the iron oxide content in cells (183–186). It is of note that *ex vivo* measurement of iron oxide content after a cell tracking experiment using EPR could also be performed to assess the biodistribution of the labeled cells (Fig. 2) and therefore complement MRI results (187).

Cell death, dilution of the iron oxides particles owing to cell proliferation and uptake of released particles by macrophages are important drawbacks of cell labeling by SPIOs (188,189). Therefore, MRI cell tracking using contrast agents may not be appropriate for rapidly dividing cells (such as cancer cells) or for the long-term monitoring of other labeled cells. In this context, reporter genes, that is, engineered genes allowing specific location and visualization of cells, can be considered as attractive because they are only expressed in living cells and are not subject to the dilution effect. The luciferase gene and the green fluorescent protein are the most common reporter genes in optical imaging. The ferritin, a paramagnetic protein involved in iron storage, has been proposed in several studies as a MRI reporter gene (190–193). This protein carries up to 4500 Fe atoms and increases the R_2 of surrounding protons (129). Unfortunately, the low sensitivity remains an issue for *in vivo* imaging (193). As the ferritin protein displays an EPR spectrum owing to its paramagnetic properties (194), the sensitive EPR spectroscopy could be potentially be used to assess the presence and expression of ferritin genes and complement MRI studies. It has been also suggested that melanin could also serve as a reporter in basic metastasis research. As the tyrosinase protein is the main enzyme involved in the synthesis of the melanin, this enzyme has been proposed as a MR reporter gene (195). An *in vitro* study has shown that breast cancer cells transfected with the tyrosinase gene displayed reduced T_1 values (196). Similar observations were also found in mouse fibroblasts and human embryonic kidney cells (197). As discussed earlier, the *in vivo* MRI contrast depends not only on the melanin content but also on the association of metals to melanin. The natural production of melanin in melanomas constitutes an attractive approach to monitor metastasis, and EPR may be used to determine the melanin content in organs with accumulation of melanoma metastases. For instance, the mouse B16 melanoma model is one of the most studied cell lines in metastasis research. Different cell subtypes have been characterized and possess different metastasis patterns. For instance, B16F10 are highly metastatic to the lungs (198) whereas another variant subline B16-F10-B2 produces brain metastasis (199). As the EPR signal intensity directly correlates with the number of melanoma cells (25), *ex vivo* X-band EPR spectroscopy constitutes a unique tool to monitor melanomas

progression to complement MRI observations (25). This would allow the quantitative assessment of the efficacy of new anti-metastatic treatments.

5. EPR AS A TOOL TO QUALIFY OR DISQUALIFY OXYGEN-SENSITIVE CONTRAST IN MRI

The oxygen level in tissues is a critical parameter in several pathologies such as stroke (48), peripheral vascular diseases (7), sepsis (49) and cancer (200). For instance, tumor hypoxia has been known for several years to promote aggressiveness, invasion and metastasis (50). In addition, low oxygen tension ($pO_2 < 5$ mmHg) affects radiotherapy efficacy and restoring an appropriate oxygenation prior to irradiation enhances the tumor radioresponse by a factor 3 (51). Hence, numerous efforts have been accomplished to improve tumor oxygenation using provascular strategies or inhibitors of oxygen consumption (201–206). Direct quantitative measurements of tumor oxygenation can be achieved by using polarographic electrodes and fibre optic probes and phosphorescence quenching based-methods such as the OxyLite system. Unfortunately, these methods are invasive and cannot be repeated on the same tissue over the time. By contrast, EPR oximetry using stable oxygen sensors can be used over long periods of time. The method requires the injection of a small amount paramagnetic probe (few crystals of lithium phthalocyanine or charcoal particles) within the tissue (29,32,207,208) and the pO_2 can be measured noninvasively using low frequency EPR systems. Oxygen, which is paramagnetic, interacts with the paramagnetic centers, inducing a shortening of the T_2 electronic relaxation time and the consequent broadening of the EPR line of the oxygen sensitive probe. More details on EPR oximetry principles and related techniques can be found in several comprehensive reviews (30,32,209). EPR oximetry has been extensively used in oncology to assess the effect of factors or pharmacological agents that modulate the tumor oxygenation (124,201,210–245). Although there are high hopes of translating EPR oximetry into the clinical arena (31,246), the present noninvasive approaches mainly rely on PET/SPECT imaging and MRI (55,56). Hypoxia imaging using PET is obtained through nitroimidazole tracers that preferentially accumulate in hypoxic cells. As this method is indirect, some radiotracers were calibrated with EPR oximetry, which provides absolute measurements of pO_2 (247–249). While these combined PET/EPR studies showed that the accumulation of compounds such as ^{18}F-FMISO, ^{18}F-EF3 and ^{18}F-FAZA in tumors was well correlated to the presence of hypoxic regions with a $pO_2 < 10$ mmHg, which is radiobiologically relevant (Fig. 3, left) , it was found that the accumulation of ^{64}Cu-ATSM in tumors involved other mechanisms independent of hypoxia (247,249). EPR has also been used to qualify and disqualify sources of MRI contrast that are sensitive to the oxygenation of the tissues. While MRI relaxometry measurements of fluorine compounds are able to provide oxygen maps that actually reflect the tissue oxygenation (250–253), these methods cannot be directly used in patients and most MRI techniques developed so far rely on the exploitation of endogenous contrast. Endogenous sources of contrast include variations of T_2* and T_1 values in tissues. T_2* is sensitive to the relative deoxyhemoglobin/oxyhemoglobin (Hb/HbO_2) ratio in vessels (254), while T_1 discloses sensitivity to dissolved paramagnetic oxygen, which acts as a T_1-shortening paramagnetic contrast agent (255).

T_2* mapping, also referred to as functional MR imaging or 'BOLD' (blood oxygen level dependent) imaging, is sensitive to variations in oxygenation in the vascular compartment. BOLD imaging has been used in many tissues to monitor changes in oxygenation and perfusion, and has been suggested in oncology as a possible biomarker of tumor hypoxia (256–261). Even if the basal T_2* values are unlikely to reflect the actual tumor pO_2 as shown in studies comparing T_2* with fiber optic measurements (260), another key question was to establish the capability of BOLD imaging to actually predict changes in tumor oxygenation induced by treatments. Several studies compared the evolution of T_2* and of the pO_2 as measured quantitatively by EPR oximetry (202,211,220,262–264). Jordan *et al.* observed that the increase in tumor oxygenation induced by carbogen or by the vasoactive agent, isosorbide dinitrate, correlated well with the evolution of the BOLD signal (211). These results were confirmed in two other tumor models where a positive correlation between R_2* values and EPR pO_2 values was observed (262,263). On the contrary, BOLD imaging failed to tackle changes in tumor oxygenation induced by the allosteric hemoglobin modifier RSR13 (220) and by the inhibitors of oxgen consumption, insulin and NS-398 (264). In other words, BOLD seems able to tackle changes in tumor oxygenation if the modulator is increasing at the same time the blood flow and the oxygenation, but cannot predict increase in oxygenation due to other factors like a decrease in oxygen consumption. This limited value of R_2* was confirmed in a meta-analysis made on tumor models that compared the respective value of possible predictive markers of response to an association irradiation/co-treatment (202). While EPR oximetry was always predictive of the issue of the anticancer treatment in these models, BOLD-MRI failed to be a predictive biomarker of response to combined treatments (202).

T_1-based techniques are sensitive to dissolved tissue oxygen and changes in tissue oxygen concentrations have been shown to produce changes in relaxation rate R_1 (=$1/T_1$) of water

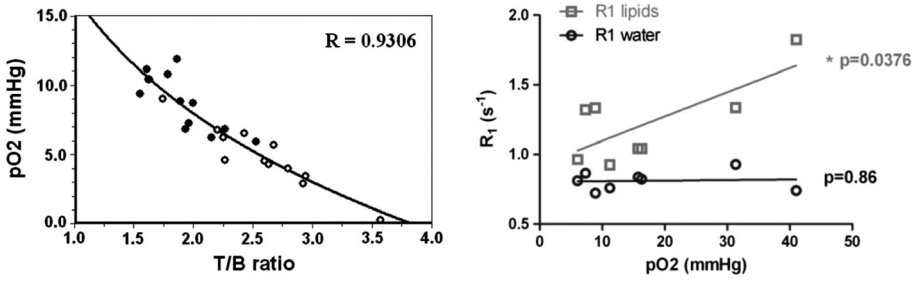

Figure 3. EPR as a tool to qualify oxygen-sensitive imaging approaches. Left: correlation between ^{18}F-FAZA tumor accumulation, as measured by microPET, and pO_2 measurements, as measured by EPR oximetry [adapted from Tran *et al.* (249)]. Right: correlation between the lipid R_1, as measured by the *MOBILE* technique, and and pO_2 measurements, as measured by EPR oximetry [adapted from Jordan *et al.* (269)].

(255,265–268). In order to counteract the lack of sensitivity of water T_1 measurements (oxygen is poorly soluble in water), Jordan *et al.* exploited the high solubility of oxygen in lipids and developed a method sensitive to T_1 variations in the lipid component of the tissues. This technique, called *MOBILE* (for mapping of oxygen by imaging lipids relaxation enhancement), was applied successfully to monitor tumor oxygenation and some ischemic models including cerebral stroke, peripheral ischemia and liver hypoxia. *MOBILE* was qualified by comparing the lipid R_1 with quantitative oxygen measurements obtained by EPR oximetry (269) (Fig. 3, right). Manipulation of the tumor oxygenation was obtained by carbogen challenge. While no correlation was obtained between the water R_1 and the pO_2 values, a significant correlation was obtained between the lipid R_1 and the pO_2 values as measured by EPR (269).

6. COMBINED EPR / MRI STUDIES OF TISSUE HEMODYNAMICS AND TISSUE ENERGETICS

In addition to the qualification of new MRI protocols, complementary information may be obtained by combining EPR and MRI. In the first examples of combination of both techniques, MRI was actually simply used to localize without ambiguity the site of the EPR oxygen sensors (210,270–272). More interestingly, EPR and MRI have been used together in a multimodality approach in order to gain complementary information on the physiological status of a tissue. We have already mentioned in the description of the contrast agents the interest for this combination to map the redox status of tissues using nitroxides as CAs. One example of successful combination involved EPR oximetry with the application of gradient echo sequences in the kidneys using models of sepsis (273). Thanks to the pO_2 EPR readings, the source of contrast in the kidneys was linked to the oxygenation status. The combination of EPR oximetry with perfusion sensitive MRI methods has been applied mainly to characterize the tumor microenvironment (124,214,221–226,236,239,243,244), helping to identify the different components to the evolution of the tumor hemodynamics by dissecting its components, the blood flow and the oxygen consumption. In addition to these components, a study carefully looked at the metabolic status of tumor areas by adding ^{1}H-MRS in order to determine the lactate concentration (274). In another study, EPR oximetry and ^{31}P NMR were used together to elucidate the complex link between the brain oxygenation and the cellular energetics (275).

The best example for combining MRI and EPR systems is by exploiting the dynamic nuclear polarization (DNP), also called the Overhauser effect, to detect free radicals. This process allows the signal enhancement of the signal of nuclear spins located in the closed vicinity of paramagnetic agents (276–278). In other words, information on free radicals can be obtained with a high anatomical resolution and a good sensitivity using NMR scanners (279). Overhauser magnetic resonance imaging (OMRI) or proton electron double resonance imaging (PEDRI) has been developed to map the spatial distribution of free radicals in living organisms (280,281). To achieve a DNP, the samples must be irradiated with an EPR irradiation pulse. To counter this possible heating by the irradiation at the resonance frequency of the free radicals, field-cycled PEDRI was developed (277). The magnetic field strength is decreased during the EPR pulse so that the irradiation frequency is kept relatively low (282), then the magnetic field is rapidly increased to gain in sensitivity for recording the NMR signal. For this type of application, paramagnetic with narrow EPR linewidth (in other words, with a relatively long T_2e) is preferred. Typically, most studies have focused on the detection of nitroxides (283) and triaryl methyl or trityl radicals (284). The method is sensitive to changes in EPR linewidths and to the interaction with proteins as shown for the nitroxides (283). Trityl radicals are less sensitive to the immobilization and their EPR linewidth vary linearly as a function of the oxygenation (284). A good example developed by the group of Krishna at the NCI was the application of OMRI to monitor tumor oxygenation coregisterd with MRI anatomy (285). Another study led by Matsumoto *et al.* showed that the OMRI technology allowed the simultaneous assessment of tissue oxygenation and microvascular permeability, parameters that were calculated through the analysis of the OMRI signal enhancement profiles. The obtained information with these techniques is promising to elucidate the link between the tumor oxygenation and the vascular permeability (286). Focusing on redox imaging, it has been demonstrated that the biodistribution, the reduction and the clearance of nitroxides could be imaged in small animals using PEDRI (34,279,287,288). OMRI techniques also allow simultaneous registration of several probes that are specific for different molecular events. For instance, Utsumi *et al.* reported the simultaneous imaging of ^{14}N- and ^{15}N-labeled nitroxides in mice. OMRI simultaneously obtained dual images of two individual chemical processes. Oxidation and reduction were monitored in a rate-dependent manner at nanometer scale by labeling membrane-permeable and -impermeable nitroxyl radicals with ^{14}N and ^{15}N nuclei. OMRI offers thus great promises for *in vivo* molecular imaging of oxidative and reductive events (289).

7. CONCLUSION

Unlike MRI, EPR remains not well known among biomedical scientists. Possible reasons for this may be the complex EPR physics, the cost of the EPR equipments and the lack of clinical applications. Maybe more importantly, the absence of accessible educational handbooks for biomedical scientists (most books start to describe EPR with the spin Hamiltonian and very long equations) makes EPR repelling and unpopular in the medical community. Nevertheless, EPR is the most straightforward technique to assess the properties and the concentrations of paramagnetic species in biological media, in cells or in tissues. We briefly summarized in this review how EPR is important for MRI experiments. This can be explained by the fact that MRI contrast is often indirect (e.g. contrast of melanin, confounding factors associated with SPIO-induced contrast) and needs to be confirmed by alternative methods. Therefore EPR, which is a sensitive technique that assess the nature and the concentration of paramagnetic molecules, gives unambiguous information to support MRI data. Combining EPR and MRI research may have important applications in the development of new MR platforms for theranostic applications and for characterizing tissues properties, as demonstrated in the characterization of the tumor microenvironment (oxygenation, hemodynamics, redox status, pH, etc.).

REFERENCES

1. Zavoisky EK. Spin-magnetic resonance in paramagnetics. J Phys Acad Sci USSR 1945; 9: 211–245.
2. Salikhov KM. The scientific work of E.K. Zavoisky. In Foundations of Modern EPR, Eaton GR, Salikhov KM (eds). World Scientific: Singapore, 1998.

3. Bloch F, Hansen WW, Packard M. Nuclear induction. Phys Rev 1946; 69: 127.
4. Purcell EM, Torrey HC, Pound RV. Resonance absorption by nuclear magnetic moments in a solid. Phys Rev 1946; 69: 37–38.
5. Lauterbur PC. Image formation by induced local interactions: examples of employing nuclear magnetic resonance. Nature 1973; 242: 190–191.
6. Feldman A, Wildman E, Bartolinini G, Piette LH. In vivo electron spin resonance in rats. Phys Med Biol 1975; 20(4): 602–612.
7. Swartz HM. History of in vivo EPR. In In Vivo EPR (ESR): Theory and Applications. KAP: New York, 2003.
8. Hoch MJR, Day AR. Imagingof paramagnetic centers in diamond. Solid St Commun 1979; 30: 211–213.
9. Eaton SS, Eaton GR. EPR imaging. In Foundations of Modern EPR, Eaton GR, Salikhov KM (eds). World Scientific: Singapore, 1998; 684–694.
10. Gallez B, Swartz HM. *In vivo* EPR: when, how and why? NMR Biomed 2004; 17(5): 223–225.
11. Kuppusamy P, Chzhan M, Zweier JL. Principles of imaging. In *In Vivo* EPR (ESR): Theory and Applications. KAP: New York, 2003; 99–152.
12. Lurie DJ, Mader K. Monitoring drug delivery processes by EPR and related techniques – principles and applications. Adv Drug Deliv Rev 2005; 57(8): 1171–1190.
13. Gallez B, Bacic G, Goda F, Jiang J, O'Hara JA, Dunn JF, Swartz HM. Use of nitroxides for assessing perfusion, oxygenation, and viability of tissues: in vivo EPR and MRI studies. Magn Reson Med 1996; 35(1): 97–106.
14. Mader K, Stosser R, Borchert HH. Detection of free radicals in living mice after inhalation of DTBN by X-band ESR. Free Radic Biol Med 1993; 14(3): 339–342.
15. Berliner JL, Fujii H. Magnetic resonance imaging of biological specimens by electron paramagnetic resonance of nitroxide spin labels. Science 1985; 227(4686): 517–519.
16. Subczynski WK, Lukiewicz S, Hyde JS. Murine in vivo L-band ESR spin-label oximetry with a loop-gap resonator. Magn Reson Med 1986; 3(5): 747–754.
17. Hutchinson JMS. Frequency and power considerations for in vivo EPR and related techniques. In Vivo EPR (ESR): Theory and Applications. KAP: New York, 2003; 41–59.
18. Krishna MC, Devasahayam N, Cook JA, Subramanian S, Kuppusamy P, Mitchell JB. Electron paramagnetic resonance for small animal imaging applications. ILAR J 2001; 42(3): 209–218.
19. Subramanian K. Frequency and power considerations for in vivo EPR and related techniques. In Vivo EPR (ESR): Theory and Applications. KAP: New York, 2003; 41–59.
20. Subramanian S, Krishna MC. Dancing with the electrons: time-domain and CW in vivo EPR imaging. Magnetic Resonance Insights 2008; 2: 43–74.
21. Subramanian S, Matsumoto K, Mitchell JB, Krishna MC. Radio frequency continuous-wave and time-domain EPR imaging and Overhauser-enhanced magnetic resonance imaging of small animals: instrumental developments and comparison of relative merits for functional imaging. NMR Biomed 2004; 17(5): 263–294.
22. Vanea E, Charlier N, Dewever J, Dinguizli M, Feron O, Baurain JF, Gallez B. Molecular electron paramagnetic resonance imaging of melanin in melanomas: a proof-of-concept. NMR Biomed 2008; 21(3): 296–300.
23. Godechal Q, Leveque P, Marot L, Baurain JF, Gallez B. Optimization of electron paramagnetic resonance imaging for visualization of human skin melanoma in various stages of invasion. Exp Dermatol 2012; 21(5): 341–346.
24. Godechal Q, Ghanem GE, Cook MG, Gallez B. Electron paramagnetic resonance spectrometry and imaging in melanomas: comparison between pigmented and nonpigmented human malignant melanomas. Mol Imag 2013; 12(4): 218–223.
25. Godechal Q, Defresne F, Danhier P, Leveque P, Porporato PE, Sonveaux P, Baurain JF, Feron O, Gallez B. Assessment of melanoma extent and melanoma metastases invasion using electron paramagnetic resonance and bioluminescence imaging. Contrast Media Mol Imag 2011; 6(4): 282–288.
26. Cesareo E, Korkina L, D'Errico G, Vitiello G, Aguzzi MS, Passarelli F, Pedersen JZ, Facchiano A. An Endogenous Electron Spin Resonance (ESR) signal discriminates nevi from melanomas in human specimens: a step forward in its diagnostic application. PLoS One 2012; 7(11): e48849.
27. Timmins GS, Liu KJ. Spin trapping in vivo: facts and artifacts. In In Vivo EPR (ESR): Theory and Applications. KAP: New York, 2003.
28. Vikram DS, Zweier JL, Kuppusamy P. Methods for noninvasive imaging of tissue hypoxia. Antioxid Redox Signal 2007; 9(10): 1745–1756.
29. Liu KJ, Gast P, Moussavi M, Norby SW, Vahidi N, Walczak T, Wu M, Swartz HM. Lithium phthalocyanine: a probe for electron paramagnetic resonance oximetry in viable biological systems. Proc Natl Acad Sci U S A 1993; 90(12): 5438–5442.
30. Krishna MC, Matsumoto S, Yasui H, Saito K, Devasahayam N, Subramanian S, Mitchell JB. Electron paramagnetic resonance imaging of tumor pO(2). Radiat Res 2012; 177(4): 376–386.
31. Khan N, Williams BB, Hou H, Li H, Swartz HM. Repetitive tissue pO2 measurements by electron paramagnetic resonance oximetry: current status and future potential for experimental and clinical studies. Antioxid Redox Signal 2007; 9(8): 1169–1182.
32. Gallez B, Baudelet C, Jordan BF. Assessment of tumor oxygenation by electron paramagnetic resonance: principles and applications. NMR Biomed 2004; 17(5): 240–262.
33. Swartz HM, Khan N, Khramtsov VV. Use of electron paramagnetic resonance spectroscopy to evaluate the redox state in vivo. Antioxid Redox Signal 2007; 9(10): 1757–1771.
34. Matsumoto K, Hyodo F, Anzai K, Utsumi H, Mitchell JB, Krishna MC. Brain redox imaging. Meth Mol Biol 2011; 711: 397–419.
35. Khramtsov VV, Grigor'ev IA, Foster MA, Lurie DJ. In vitro and in vivo measurement of pH and thiols by EPR-based techniques. Antioxid Redox Signal 2004; 6(3): 667–676.
36. Gallez B, Mader K, Swartz HM. Noninvasive measurement of the pH inside the gut by using pH-sensitive nitroxides. An in vivo EPR study Magn Reson Med 1996; 36(5): 694–697.
37. Driesschaert B, Marchand V, Leveque P, Gallez B, Marchand-Brynaert J. A phosphonated triarylmethyl radical as a probe for measurement of pH by EPR. Chem Commun (Camb) 2012; 48(34): 4049–4051.
38. Dhimitruka I, Bobko AA, Eubank TD, Komarov DA, Khramtsov VV. Phosphonated trityl probes for concurrent in vivo tissue oxygen and pH monitoring using electron paramagnetic resonance-based techniques. J Am Chem Soc 2013; 135(15): 5904–5910.
39. Kempe S, Metz H, Mader K. Application of electron paramagnetic resonance (EPR) spectroscopy and imaging in drug delivery research – chances and challenges. Eur J Pharm Biopharm 2010; 74(1): 55–66.
40. Halpern HJ, Chandramouli GV, Barth ED, Yu C, Peric M, Grdina DJ, Teicher BA. Diminished aqueous microviscosity of tumors in murine models measured with in vivo radiofrequency electron paramagnetic resonance. Cancer Res 1999; 59(22): 5836–5841.
41. Symons MCR. The detection and characterization of free radical species. In Techniques in Free Radical Research. Elsevier: Amsterdam, 1991.
42. Dunn JF, Swartz H. Combining NMR and EPR/ESR for in vivo experiments. In *In Vivo* EPR (ESR): Theory and Applications. KAP: New York, 2003; 579–597.
43. Laurent S, Vander Elst L, Henoumont C, Muller RN. How to measure the transmetallation of a gadolinium complex. Contrast Media Mol Imag 2010; 5(6): 305–308.
44. Burtea C, Laurent S, Vander Elst L, Muller RN. Contrast agents: magnetic resonance. Handb Exp Pharmacol 2008; 185 Pt 1: 135–165.
45. Tóth É, Helm L, Merbach AE, Hedinger R, Hegetschweiler K, Jánossy A. Structure and dynamics of a trinuclear gadolinium(III) complex: the effect of intramolecular electron spin relaxation on its proton relaxivity. Inorg Chem 1998; 37(16): 4104–4113.
46. Borel A, Kang H, Gateau C, Mazzanti M, Clarkson RB, Belford RL. Variable temperature and EPR frequency study of two aqueous Gd(III) complexes with unprecedented sharp lines. J Phys Chem A 2006; 110(45): 12434–12438.
47. Borel A, Helm L, Merbach AE. Molecular dynamics simulations of MRI-relevant GdIII chelates: direct access to outer-sphere relaxivity. Chemistry 2001; 7(3): 600–610.
48. Borel A, Bean JF, Clarkson RB, Helm L, Moriggi L, Sherry AD, Woods M. Towards the rational design of MRI contrast agents: electron spin relaxation is largely unaffected by the coordination geometry of gadolinium(III)-DOTA-type complexes. Chemistry 2008; 14(9): 2658–2667.
49. Nicolle GM, Toth E, Schmitt-Willich H, Raduchel B, Merbach AE. The impact of rigidity and water exchange on the relaxivity of a dendritic MRI contrast agent. Chemistry 2002; 8(5): 1040–1048.
50. Laus S, Ruloff R, Toth E, Merbach AE. GdIII complexes with fast water exchange and high thermodynamic stability: potential building blocks for high-relaxivity MRI contrast agents. Chemistry 2003; 9(15): 3555–3566.

51. Andre JP, Maecke HR, Toth E, Merbach AA. Synthesis and physicochemical characterization of a novel precursor for covalently bound macromolecular MRI contrast agents. J Biol Inorg Chem 1999; 4(3): 341–347.
52. Borel A, Yerly F, Helm L, Merbach AE. Multiexponential electronic spin relaxation and Redfield's limit in Gd(III) complexes in solution: consequences for 17O/1H NMR and EPR simultaneous analysis. J Am Chem Soc 2002; 124(9): 2042–2048.
53. Benmelouka M, Van Tol J, Borel A, Port M, Helm L, Brunel LC, Merbach AE. A high-frequency EPR study of frozen solutions of Gd(III) complexes: straightforward determination of the zero-field splitting parameters and simulation of the NMRD profiles. J Am Chem Soc 2006; 128(24): 7807–7816.
54. Zhou X, Caravan P, Clarkson RB, Westlund PO. On the philosophy of optimizing contrast agents. An analysis of 1H NMRD profiles and ESR lineshapes of the Gd(III)complex MS–325 + HSA. J Magn Reson 2004; 167(1): 147–160.
55. Rast S, Borel A, Helm L, Belorizky E, Fries PH, Merbach AE. EPR spectroscopy of MRI-related Gd(III) complexes: simultaneous analysis of multiple frequency and temperature spectra, including static and transient crystal field effects. J Am Chem Soc 2001; 123(11): 2637–2644.
56. Benmelouka M, Borel A, Moriggi L, Helm L, Merbach AE. Design of Gd(III)-based magnetic resonance imaging contrast agents: static and transient zero-field splitting contributions to the electronic relaxation and their impact on relaxivity. J Phys Chem B 2007; 111(4): 832–840.
57. Platas-Iglesias C, Vander Elst L, Zhou W, Muller RN, Geraldes CF, Maschmeyer T, Peters JA. Zeolite GdNaY nanoparticles with very high relaxivity for application as contrast agents in magnetic resonance imaging. Chemistry 2002; 8(22): 5121–5131.
58. Vuong QL, Van Doorslaer S, Bridot JL, Argante C, Alejandro G, Hermann R, Disch S, Mattea C, Stapf S, Gossuin Y. Paramagnetic nanoparticles as potential MRI contrast agents: characterization, NMR relaxation, simulations and theory. MAGMA 2012; 25(6): 467–478.
59. Smirnova TI, Smirnov AI, Belford RL, Clarkson RB. Interaction of Gd (III) MRI contrast agents with membranes: a review of recent EPR studies. MAGMA 1999; 8(3): 214–229.
60. Lagerstedt JO, Petrlova J, Hilt S, Marek A, Chung Y, Sriram R, Budamagunta MS, Desreux JF, Thonon D, Jue T, Smirnov AI, Voss JC. EPR assessment of protein sites for incorporation of Gd(III) MRI contrast labels. Contrast Media Mol Imag 2013; 8(3): 252–264.
61. Luciani A, Olivier JC, Clement O, Siauve N, Brillet PY, Bessoud B, Gazeau F, Uchegbu IF, Kahn E, Frija G, Cuenod CA. Glucose-receptor MR imaging of tumors: study in mice with PEGylated paramagnetic niosomes. Radiology 2004; 231(1): 135–142.
62. Takeshita K, Kinoshita S, Okazaki S. Simple method for quantification of gadolinium magnetic resonance imaging contrast agents using ESR spectroscopy. Chem Pharm Bull (Tokyo) 2012; 60(1): 31–36.
63. Strijkers GJ, Mulder WJ, van Tilborg GA, Nicolay K. MRI contrast agents: current status and future perspectives. Anticancer Agents Med Chem 2007; 7(3): 291–305.
64. Eschenko O, Evrard HC, Neves RM, Beyerlein M, Murayama Y, Logothetis NK. Tracing of noradrenergic projections using manganese-enhanced MRI. Neuroimage 2012; 59(4): 3252–3265.
65. Silva AC, Bock NA. Manganese-enhanced MRI: an exceptional tool in translational neuroimaging. Schizophr Bull 2008; 34(4): 595–604.
66. Pautler R, Silva A, Koretsky A. In vivo neuronal tract tracing using manganese-enhanced magnetic resonance imaging. Magn Reson Med 1998; 40(5): 740–748.
67. Inoue T, Majid T, Pautler RG. Manganese enhanced MRI (MEMRI): neurophysiological applications. Rev Neurosci 2011; 22(6): 675–694.
68. Rivera-Mancia S, Rios C, Montes S. Manganese accumulation in the CNS and associated pathologies. Biometals 2011; 24(5): 811–825.
69. Roth J, Ponzoni S, Aschner M. Manganese homeostasis and transport. Metal Ions Life Sci 2013; 12: 169–201.
70. Dorman DC, Struve MF, Wong BA, Dye JA, Robertson ID. Correlation of brain magnetic resonance imaging changes with pallidal manganese concentrations in rhesus monkeys following subchronic manganese inhalation. Toxicol Sci 2006; 92(1): 219–227.
71. Gallez B, Demeure R, Baudelet C, Abdelouahab N, Beghein N, Jordan B, Geurts M, Roels HA. Non invasive quantification of manganese deposits in the rat brain by local measurement of NMR proton T1 relaxation times. Neurotoxicology 2001; 22(3): 387–392.
72. Reimer P, Schneider G, Schima W. Hepatobiliary contrast agents for contrast-enhanced MRI of the liver: properties, clinical development and applications. Eur Radiol 2004; 14(4): 559–578.
73. Gallez B, Bacic G, Swartz HM. Evidence for the dissociation of the hepatobiliary MRI contrast agent Mn-DPDP. Magn Reson Med 1996; 35(1): 14–19.
74. Schmidt PP, Toft KG, Skotland T, Andersson K. Stability and transmetallation of the magnetic resonance contrast agent MnDPDP measured by EPR. J Biol Inorg Chem 2002; 7(3): 241–248.
75. Hustvedt SO, Grant D, Southon TE, Zech K. Plasma pharmacokinetics, tissue distribution and excretion of MnDPDP in the rat and dog after intravenous administration. Acta Radiol 1997; 38(4 Pt 2): 690–699.
76. Colet JM, Vander Elst L, Muller RN. Dynamic evaluation of the hepatic uptake and clearance of manganese-based MRI contrast agents: a 31P NMR study on the isolated and perfused rat liver. J Magn Reson Imag 1998; 8(3): 663–669.
77. Gallez B, Baudelet C, Adline J, Charbon V, Lambert DM. The uptake of Mn-DPDP by hepatocytes is not mediated by the facilitated transport of pyridoxine. Magn Reson Imag 1996; 14(10): 1191–1195.
78. Gallez B, Baudelet C, Adline J, Geurts M, Delzenne N. Accumulation of manganese in the brain of mice after intravenous injection of manganese-based contrast agents. Chem Res Toxicol 1997; 10(4): 360–363.
79. Gallez B, Baudelet C, Geurts M. Regional distribution of manganese found in the brain after injection of a single dose of manganese-based contrast agents. Magn Reson Imag 1998; 16(10): 1211–1215.
80. Misselwitz B, Muhler A, Weinmann HJ. A toxicologic risk for using manganese complexes? A literature survey of existing data through several medical specialties. Invest Radiol 1995; 30(10): 611–620.
81. Rosen GM, Griffeth LK, Brown MA, Drayer BP. Intrathecal administration of nitroxides as potential contrast agents for MR imaging. Radiology 1987; 163(1): 239–243.
82. Brasch RC, Nitecki DE, Brant-Zawadzki M, Enzmann DR, Wesbey GE, Tozer TN, Tuck LD, Cann CE, Fike JR, Sheldon P. Brain nuclear magnetic resonance imaging enhanced by a paramagnetic nitroxide contrast agent: preliminary report. AJR Am J Roentgenol 1983; 141(5): 1019–1023.
83. Brasch RC. Work in progress: methods of contrast enhancement for NMR imaging and potential applications. A subject review Radiology 1983; 147(3): 781–788.
84. Winalski CS, Shortkroff S, Mulkern RV, Schneider E, Rosen GM. Magnetic resonance relaxivity of dendrimer-linked nitroxides. Magn Reson Med 2002; 48(6): 965–972.
85. Gallez B, Lacour V, Demeure R, Debuyst R, Dejehet F, De Keyser JL, Dumont P. Spin labelled arabinogalactan as MRI contrast agent. Magn Reson Imag 1994; 12(1): 61–69.
86. Gallez B, Debuyst R, Dejehet F, Keyser JL, Lacour V, Demeure R, Dumont P. Relaxivity and molecular dynamics of spin labeled polysaccharides. Magn Reson Mater Phys Biol Med 1994; 2(1): 61–68.
87. Chan HC, Sun KQ, Magin RL, Swartz HM. Potential of albumin labeled with nitroxides as a contrast agent for magnetic resonance imaging and spectroscopy. Bioconjug Chem 1990; 1(1): 32–36.
88. Rajca A, Wang Y, Boska M, Paletta JT, Olankitwanit A, Swanson MA, Mitchell DG, Eaton SS, Eaton GR, Rajca S. Organic radical contrast agents for magnetic resonance imaging. J Am Chem Soc 2012; 134(38): 15724–15727.
89. Vallet P, Van Haverbeke Y, Bonnet PA, Subra G, Chapat JP, Muller RN. Relaxivity enhancement of low molecular weight nitroxide stable free radicals: importance of structure and medium. Magn Reson Med 1994; 32(1): 11–15.
90. Gallez B, Demeure R, Debuyst R, Leonard D, Dejehet F, Dumont P. Evaluation of nonionic nitroxyl lipids as potential organ-specific contrast agents for magnetic resonance imaging. Magn Reson Imag 1992; 10(3): 445–455.
91. Gallez B, Debuyst R, Demeure R, Dejehet F, Grandin C, Van Beers B, Taper H, Pringot J, Dumont P. Evaluation of a nitroxyl fatty acid as liver contrast agent for magnetic resonance imaging. Magn Reson Med 1993; 30(5): 592–599.
92. Bennett HF, Brown RD, 3rd, Keana JF, Koenig SH, Swartz HM. Interactions of nitroxides with plasma and blood: effect on 1/T1 of water protons. Magn Reson Med 1990; 14(1): 40–55.
93. Bennett HF, Brown RD, 3rd, Koenig SH, Swartz HM. Effects of nitroxides on the magnetic field and temperature dependence of 1/T1 of solvent water protons. Magn Reson Med 1987; 4(2): 93–111.

94. Swartz HM, Chen K, Pals M, Sentjurc M, Morse PD, 2nd. Hypoxia-sensitive NMR contrast agents. Magn Reson Med 1986; 3(1): 169–174.
95. Keana JF, Van Nice FL. Influence of structure on the reduction of nitroxide MRI contrast-enhancing agents by ascorbate. Physiol Chem Phys Med NMR 1984; 16(6): 477–480.
96. Iannone A, Tomasi A, Vannini V, Swartz HM. Metabolism of nitroxide spin labels in subcellular fraction of rat liver. I. Reduction by microsomes. Biochim Biophys Acta 1990; 1034(3): 285–289.
97. Iannone A, Tomasi A, Vannini V, Swartz HM. Metabolism of nitroxide spin labels in subcellular fractions of rat liver. II. Reduction in the cytosol. Biochim Biophys Acta 1990; 1034(3): 290–293.
98. Iannone A, Hu HP, Tomasi A, Vannini V, Swartz HM. Metabolism of aqueous soluble nitroxides in hepatocytes: effects of cell integrity, oxygen, and structure of nitroxides. Biochim Biophys Acta 1989; 991(1): 90–96.
99. Couet WR, Brasch RC, Sosnovsky G, Tozer TN. Factors affecting nitroxide reduction in ascorbate solution and tissue homogenates. Magn Reson Imag 1985; 3(1): 83–88.
100. Swartz HM. Use of nitroxides to measure redox metabolism in cells and tissues. J Chem Soc Faraday Trans 1: Phys Chem Condensed Phases 1987; 83(1): 191–202.
101. Pals MA, Swartz HM. Oxygen-dependent metabolism of potential magnetic resonance contrast agents. Invest Radiol 1987; 22(6): 497–501.
102. Chen K, Glockner JF, Morse PD, 2nd, Swartz HM. Effects of oxygen on the metabolism of nitroxide spin labels in cells. Biochemistry 1989; 28(6): 2496–2501.
103. Kuppusamy P, Li H, Ilangovan G, Cardounel AJ, Zweier JL, Yamada K, Krishna MC, Mitchell JB. Noninvasive imaging of tumor redox status and its modification by tissue glutathione levels. Cancer Res 2002; 62(1): 307–312.
104. Yamada KI, Kuppusamy P, English S, Yoo J, Irie A, Subramanian S, Mitchell JB, Krishna MC. Feasibility and assessment of noninvasive in vivo redox status using electron paramagnetic resonance imaging. Acta Radiol 2002; 43(4): 433–440.
105. Ilangovan G, Li H, Zweier JL, Kuppusamy P. In vivo measurement of tumor redox environment using EPR spectroscopy. Mol Cell Biochem 2002; 234–235(1–2): 393–398.
106. Matsumoto K, Hyodo F, Matsumoto A, Koretsky AP, Sowers AL, Mitchell JB, Krishna MC. High-resolution mapping of tumor redox status by magnetic resonance imaging using nitroxides as redox-sensitive contrast agents. Clin Cancer Res 2006; 12(8): 2455–2462.
107. Hyodo F, Soule BP, Matsumoto K, Matusmoto S, Cook JA, Hyodo E, Sowers AL, Krishna MC, Mitchell JB. Assessment of tissue redox status using metabolic responsive contrast agents and magnetic resonance imaging. J Pharm Pharmacol 2008; 60(8): 1049–1060.
108. Fujii H, Sato-Akaba H, Kawanishi K, Hirata H. Mapping of redox status in a brain-disease mouse model by three-dimensional EPR imaging. Magn Reson Med 2011; 65(1): 295–303.
109. Hyodo F, Matsumoto K, Matsumoto A, Mitchell JB, Krishna MC. Probing the intracellular redox status of tumors with magnetic resonance imaging and redox-sensitive contrast agents. Cancer Res 2006; 66(20): 9921–9928.
110. Hyodo F, Chuang KH, Goloshevsky AG, Sulima A, Griffiths GL, Mitchell JB, Koretsky AP, Krishna MC. Brain redox imaging using blood-brain barrier-permeable nitroxide MRI contrast agent. J Cereb Blood Flow Metab 2008; 28(6): 1165–1174.
111. Matsumoto K, Hyodo F, Matsumoto A, Koretsky AP, Sowers AL, Mitchell JB, Krishna MC. High-resolution mapping of tumor redox status by magnetic resonance imaging using nitroxides as redox-sensitive contrast agents. Clin Cancer Res 2006; 12(8): 2455–2462.
112. Davis RM, Matsumoto S, Bernardo M, Sowers A, Matsumoto K, Krishna MC, Mitchell JB. Magnetic resonance imaging of organic contrast agents in mice: capturing the whole-body redox landscape. Free Radic Biol Med 2011; 50(3): 459–468.
113. Caia GL, Efimova OV, Velayutham M, El-Mahdy MA, Abdelghany TM, Kesselring E, Petryakov S, Sun Z, Samouilov A, Zweier JL. Organ specific mapping of in vivo redox state in control and cigarette smoke-exposed mice using EPR/NMR co-imaging. J Magn Reson 2012; 216: 21–27.
114. Eriksson UG, Ogan MD, Peng CT, Brasch RC, Tozer TN. Metabolic fate in the dog of the nitroxide moiety in a compound with potential utility as a contrast agent in MRI. Magn Reson Med 1987; 5(1): 73–77.
115. Eriksson UG, Schuhmann G, Brasch RC, Tozer TN. Pharmacokinetics in the rat and the dog of a nonionic nitroxide contrast agent for magnetic resonance imaging. J Pharm Sci 1988; 77(2): 97–103.
116. Liebmann J, Bourg J, Krishna CM, Glass J, Cook JA, Mitchell JB. Pharmacokinetic properties of nitroxide-labeled albumin in mice. Life Sci 1994; 54(26): PL503–509.
117. Grant CW, Barber KR, Florio E, Karlik S. A phospholipid spin label used as a liposome-associated MRI contrast agent. Magn Reson Med 1987; 5(4): 371–376.
118. Yokoyama H, Itoh O, Ogata T, Obara H, Ohya-Nishiguchi H, Kamada H. Temporal brain imaging by a rapid scan ESR-CT system in rats receiving intraperitoneal injection of a methyl ester nitroxide radical. Magn Reson Imag 1997; 15(9): 1079–1084.
119. Yokoyama H, Itoh O, Aoyama M, Obara H, Ohya H, Kamada H. In vivo temporal EPR imaging of the brain of rats by using two types of blood-brain barrier-permeable nitroxide radicals. Magn Reson Imag 2002; 20(3): 277–284.
120. Shen J, Liu S, Miyake M, Liu W, Pritchard A, Kao JP, Rosen GM, Tong Y, Liu KJ. Use of 3-acetoxymethoxycarbonyl-2,2,5,5-tetramethyl-1-pyrrolidinyloxyl as an EPR oximetry probe: potential for in vivo measurement of tissue oxygenation in mouse brain. Magn Reson Med 2006; 55(6): 1433–1440.
121. Miyake M, Shen J, Liu S, Shi H, Liu W, Yuan Z, Pritchard A, Kao JP, Liu KJ, Rosen GM. Acetoxymethoxycarbonyl nitroxides as electron paramagnetic resonance proimaging agents to measure O2 levels in mouse brain: a pharmacokinetic and pharmacodynamic study. J Pharmacol Exp Ther 2006; 318(3): 1187–1193.
122. Miyake M, Burks SR, Weaver J, Tsai P, Liu W, Bigio D, Bauer KS, Liu KJ, Rosen GM, Kao JP. Comparison of two nitroxide labile esters for delivering electron paramagnetic resonance probes into mouse brain. J Pharm Sci 2010; 99(8): 3594–3600.
123. Fujii HG, Sato-Akaba H, Emoto MC, Itoh K, Ishihara Y, Hirata H. Noninvasive mapping of the redox status in septic mouse by in vivo electron paramagnetic resonance imaging. Magn Reson Imag 2013; 31(1): 130–138.
124. Goda F, Bacic G, O'Hara JA, Gallez B, Swartz HM, Dunn JF. The relationship between partial pressure of oxygen and perfusion in two murine tumors after X-ray irradiation: a combined gadopentetate dimeglumine dynamic magnetic resonance imaging and in vivo electron paramagnetic resonance oximetry study. Cancer Res 1996; 56(14): 3344–3349.
125. Laurent S, Forge D, Port M, Roch A, Robic C, Vander Elst L, Muller RN. Magnetic iron oxide nanoparticles: synthesis, stabilization, vectorization, physicochemical characterizations, and biological applications. Chem Rev 2008; 108(6): 2064–2110.
126. Van Beers BE, Gallez B, Pringot J. Contrast-enhanced MR imaging of the liver. Radiology 1997; 203(2): 297–306.
127. Tanimoto A, Kuribayashi S. Application of superparamagnetic iron oxide to imaging of hepatocellular carcinoma. Eur J Radiol 2006; 58(2): 200–216.
128. Kudo M. Diagnostic imaging of hepatocellular carcinoma: recent progress. Oncology 2011; 81(Suppl 1): 73–85.
129. Gossuin Y, Gillis P, Hocq A, Vuong QL, Roch A. Magnetic resonance relaxation properties of superparamagnetic particles. Wiley Interdiscip Rev Nanomed Nanobiotechnol 2009; 1(3): 299–310.
130. Wang YX, Hussain SM, Krestin GP. Superparamagnetic iron oxide contrast agents: physicochemical characteristics and applications in MR imaging. Eur Radiol 2001; 11(11): 2319–2331.
131. Islam T, Wolf G. The pharmacokinetics of the lymphotropic nanoparticle MRI contrast agent ferumoxtran-10. Cancer Biomark 2009; 5(2): 69–73.
132. Harnan SE, Cooper KL, Meng Y, Ward SE, Fitzgerald P, Papaioannou D, Ingram C, Lorenz E, Wilkinson ID, Wyld L. Magnetic resonance for assessment of axillary lymph node status in early breast cancer: a systematic review and meta-analysis. Eur J Surg Oncol 2011; 37(11): 928–936.
133. Wu L, Cao Y, Liao C, Huang J, Gao F. Diagnostic performance of USPIO-enhanced MRI for lymph-node metastases in different body regions: a meta-analysis. Eur J Radiol 2011; 80(2): 582–589.
134. Tassa C, Shaw SY, Weissleder R. Dextran-coated iron oxide nanoparticles: a versatile platform for targeted molecular imaging, molecular diagnostics, and therapy. Acc Chem Res 2011; 44(10): 842–852.
135. Fattahi H, Laurent S, Liu F, Arsalani N, Vander Elst L, Muller RN. Magnetoliposomes as multimodal contrast agents for molecular imaging and cancer nanotheragnostics. Nanomedicine (Lond) 2011; 6(3): 529–544.
136. Liu F, Laurent S, Fattahi H, Vander Elst L, Muller RN. Superparamagnetic nanosystems based on iron oxide nanoparticles for biomedical imaging. Nanomedicine (Lond) 2011; 6(3): 519–528.

137. Yigit MV, Moore A, Medarova Z. Magnetic nanoparticles for cancer diagnosis and therapy. Pharm Res 2012; 29(5): 1180–1188.
138. Xu C, Sun S. New forms of superparamagnetic nanoparticles for biomedical applications. Adv Drug Deliv Rev 2013; 65(5): 732–743.
139. Weissleder R, Stark DD, Engelstad BL, Bacon BR, Compton CC, White DL, Jacobs P, Lewis J. Superparamagnetic iron oxide: pharmacokinetics and toxicity. AJR Am J Roentgenol 1989; 152(1): 167–173.
140. Neuwelt EA, Hamilton BE, Varallyay CG, Rooney WR, Edelman RD, Jacobs PM, Watnick SG. Ultrasmall superparamagnetic iron oxides (USPIOs): a future alternative magnetic resonance (MR) contrast agent for patients at risk for nephrogenic systemic fibrosis (NSF)? Kidney Int 2009; 75(5): 465–474.
141. Singh N, Jenkins GJ, Asadi R, Doak SH. Potential toxicity of superparamagnetic iron oxide nanoparticles (SPION). Nano Rev 2010; 1: 5358. DOI: 10.3402/nano.v1i0.5358
142. Soenen SJ, Himmelreich U, Nuytten N, De Cuyper M. Cytotoxic effects of iron oxide nanoparticles and implications for safety in cell labelling. Biomaterials 2011; 32(1): 195–205.
143. Mahmoudi M, Laurent S, Shokrgozar MA, Hosseinkhani M. Toxicity evaluations of superparamagnetic iron oxide nanoparticles: cell 'vision' versus physicochemical properties of nanoparticles. ACS Nano 2011; 5(9): 7263–7276.
144. Laurent S, Burtea C, Thirifays C, Hafeli UO, Mahmoudi M. Crucial ignored parameters on nanotoxicology: the importance of toxicity assay modifications and 'cell vision'. PLoS One 2012; 7(1): e29997.
145. Liu G, Gao J, Ai H, Chen X. Applications and potential toxicity of magnetic iron oxide nanoparticles. Small 2013; 9(9–10): 1533–1545.
146. van den Bos EJ, Baks T, Moelker AD, Kerver W, van Geuns RJ, van der Giessen WJ, Duncker DJ, Wielopolski PA. Magnetic resonance imaging of haemorrhage within reperfused myocardial infarcts: possible interference with iron oxide-labelled cell tracking? Eur Heart J 2006; 27(13): 1620–1626.
147. Himmelreich U, Dresselaers T. Cell labeling and tracking for experimental models using magnetic resonance imaging. Methods 2009; 48(2): 112–124.
148. Schroeter M, Saleh A, Wiedermann D, Hoehn M, Jander S. Histochemical detection of ultrasmall superparamagnetic iron oxide (USPIO) contrast medium uptake in experimental brain ischemia. Magn Reson Med 2004; 52(2): 403–406.
149. Boutry S, Forge D, Burtea C, Mahieu I, Murariu O, Laurent S, Vander Elst L, Muller RN. How to quantify iron in an aqueous or biological matrix: a technical note. Contrast Media Mol Imag 2009; 4(6): 299–304.
150. Yancy AD, Olzinski AR, Hu TC, Lenhard SC, Aravindhan K, Gruver SM, Jacobs PM, Willette RN, Jucker BM. Differential uptake of ferumoxtran-10 and ferumoxytol, ultrasmall superparamagnetic iron oxide contrast agents in rabbit: critical determinants of atherosclerotic plaque labeling. J Magn Reson Imag 2005; 21(4): 432–442.
151. Huang C, Neoh KG, Wang L, Kang ET, Shuter B. Surface functionalization of superparamagnetic nanoparticles for the development of highly efficient magnetic resonance probe for macrophages. Contrast Media Mol Imag 2011; 6(4): 298–307.
152. Dadashzadeh ER, Hobson M, Henry Bryant L, Jr, Dean DD, Frank JA. Rapid spectrophotometric technique for quantifying iron in cells labeled with superparamagnetic iron oxide nanoparticles: potential translation to the clinic. Contrast Media Mol Imag 2013; 8(1): 50–56.
153. Levy M, Luciani N, Alloyeau D, Elgrabli D, Deveaux V, Pechoux C, Chat S, Wang G, Vats N, Gendron F, Factor C, Lotersztajn S, Luciani A, Wilhelm C, Gazeau F. Long term in vivo biotransformation of iron oxide nanoparticles. Biomaterials 2011; 32(16): 3988–3999.
154. Radermacher KA, Beghein N, Boutry S, Laurent S, Vander Elst L, Muller RN, Jordan BF, Gallez B. In vivo detection of inflammation using pegylated iron oxide particles targeted at E-selectin: a multimodal approach using MR imaging and EPR spectroscopy. Invest Radiol 2009; 44(7): 398–404.
155. Chertok B, Cole AJ, David AE, Yang VC. Comparison of electron spin resonance spectroscopy and inductively-coupled plasma optical emission spectroscopy for biodistribution analysis of iron-oxide nanoparticles. Mol Pharm 2010; 7(2): 375–385.
156. Fujii H, Yoshikawa K, Berliner LJ. In vivo fate of superparamagnetic iron oxides during sepsis. Magn Reson Imag 2002; 20(3): 271–276.
157. Radermacher KA, Boutry S, Laurent S, Elst LV, Mahieu I, Bouzin C, Magat J, Gregoire V, Feron O, Muller RN, Jordan BF, Gallez B. Iron oxide particles covered with hexapeptides targeted at phosphatidylserine as MR biomarkers of tumor cell death. Contrast Media Mol Imag 2010; 5(5): 258–267.
158. Radermacher KA, Magat J, Bouzin C, Laurent S, Dresselaers T, Himmelreich U, Boutry S, Mahieu I, Vander Elst L, Feron O, Muller RN, Jordan BF, Gallez B. Multimodal assessment of early tumor response to chemotherapy: comparison between diffusion-weighted MRI, 1H-MR spectroscopy of choline and USPIO particles targeted at cell death. NMR Biomed 2012; 25(4): 514–522.
159. Bulte JW, Brooks RA, Moskowitz BM, Bryant LH, Jr, Frank JA. Relaxometry and magnetometry of the MR contrast agent MION-46 L. Magn Reson Med 1999; 42(2): 379–384.
160. Brenner M, Hearing VJ. The protective role of melanin against UV damage in human skin. Photochem Photobiol 2008; 84(3): 539–549.
161. Jerant AF, Johnson JT, Sheridan CD, Caffrey TJ. Early detection and treatment of skin cancer. Am Fam Physician 2000; 62(2): 357–368.
162. Balch CM, Soong SJ, Gershenwald JE, Thompson JF, Reintgen DS, Cascinelli N, Urist M, McMasters KM, Ross MI, Kirkwood JM, Atkins MB, Thompson JA, Coit DG, Byrd D, Desmond R, Zhang Y, Liu PY, Lyman GH, Morabito A. Prognostic factors analysis of 17,600 melanoma patients: validation of the American Joint Committee on Cancer melanoma staging system. J Clin Oncol 2001; 19(16): 3622–3634.
163. Herman C. Emerging technologies for the detection of melanoma: achieving better outcomes. Clin Cosmet Investig Dermatol 2012; 5: 195–212.
164. Wong SL, Balch CM, Hurley P, Agarwala SS, Akhurst TJ, Cochran A, Cormier JN, Gorman M, Kim TY, McMasters KM, Noyes RD, Schuchter LM, Valsecchi ME, Weaver DL, Lyman GH. Sentinel lymph node biopsy for melanoma: American Society of Clinical Oncology and Society of Surgical Oncology joint clinical practice guideline. Ann Surg Oncol 2012; 19(11): 3313–3324.
165. Godechal Q, Gallez B. The contribution of electron paramagnetic resonance to melanoma research. J Skin Cancer 2011; 2011: 273280.
166. Premkumar A, Marincola F, Taubenberger J, Chow C, Venzon D, Schwartzentruber D. Metastatic melanoma: correlation of MRI characteristics and histopathology. J Magn Reson Imag 1996; 6(1): 190–194.
167. Maurer J, Knollmann FD, Schlums D, Garbe C, Vogl TJ, Bier J, Felix R. Role of high-resolution magnetic resonance imaging for differentiating melanin-containing skin tumors. Invest Radiol 1995; 30(11): 638–643.
168. Maurer J, Schlums D, Knollmann FD, Garbe C, Vogl TJ, Bier J, Felix R. Failure of gadopentetate dimeglumine-enhanced, high-resolution magnetic resonance imaging to differentiate among melanin-containing skin tumors. Acad Radiol 1996; 3(3): 186–191.
169. Isiklar I, Leeds NE, Fuller GN, Kumar AJ. Intracranial metastatic melanoma: correlation between MR imaging characteristics and melanin content. AJR Am J Roentgenol 1995; 165(6): 1503–1512.
170. Enochs WS, Petherick P, Bogdanova A, Mohr U, Weissleder R. Paramagnetic metal scavenging by melanin: MR imaging. Radiology 1997; 204(2): 417–423.
171. Seiler T, Bende T, Schilling A, Wollensak J. Magnetic resonance tomography in ophthalmology. I. Choroid melanoma. Klin Monbl Augenheilkd 1987; 191(3): 203–210.
172. Godechal Q, Mignion L, Karroum O, Magat J, Danhier P, Morandini R, Ghanem GE, Leveque P, Gallez B. Influence of paramagnetic melanin on the MRI contrast in melanoma: a combined high-field (11.7 T) MRI and EPR study. Contrast Media Mol Imag 2014; 9(2): 154–160.
173. Janowski M, Bulte JW, Walczak P. Personalized nanomedicine advancements for stem cell tracking. Adv Drug Deliv Rev 2012; 64(13): 1488–1507.
174. Song HT, Jordan EK, Lewis BK, Liu W, Ganjei J, Klaunberg B, Despres D, Palmieri D, Frank JA. Rat model of metastatic breast cancer monitored by MRI at 3 tesla and bioluminescence imaging with histological correlation. J Transl Med 2009; 7: 88.
175. Townson JL, Ramadan SS, Simedrea C, Rutt BK, MacDonald IC, Foster PJ, Chambers AF. Three-dimensional imaging and quantification of both solitary cells and metastases in whole mouse liver by magnetic resonance imaging. Cancer Res 2009; 69(21): 8326–8331.
176. Heyn C, Ronald JA, Ramadan SS, Snir JA, Barry AM, MacKenzie LT, Mikulis DJ, Palmieri D, Bronder JL, Steeg PS, Yoneda T, MacDonald IC, Chambers AF, Rutt BK, Foster PJ. In vivo MRI of cancer cell fate at the single-cell level in a mouse model of breast cancer metastasis to the brain. Magn Reson Med 2006; 56(5): 1001–1010.
177. Kim JB, Urban K, Cochran E, Lee S, Ang A, Rice B, Bata A, Campbell K, Coffee R, Gorodinsky A, Lu Z, Zhou H, Kishimoto TK, Lassota P. Non-invasive detection of a small number of bioluminescent cancer cells in vivo. PLoS One 2010; 5(2): e9364.

178. Shapiro EM, Skrtic S, Sharer K, Hill JM, Dunbar CE, Koretsky AP. MRI detection of single particles for cellular imaging. Proc Natl Acad Sci U S A 2004; 101(30): 10901–10906.
179. Foster-Gareau P, Heyn C, Alejski A, Rutt BK. Imaging single mammalian cells with a 1.5 T clinical MRI scanner. Magn Reson Med 2003; 49(5): 968–971.
180. Sykova E, Jendelova P, Herynek V. Magnetic resonance imaging of stem cell migration. Methods Mol Biol 2011; 750: 79–90.
181. Mahmoudi M, Hosseinkhani H, Hosseinkhani M, Boutry S, Simchi A, Journeay WS, Subramani K, Laurent S. Magnetic resonance imaging tracking of stem cells in vivo using iron oxide nanoparticles as a tool for the advancement of clinical regenerative medicine. Chem Rev 2011; 111(2): 253–280.
182. Bulte JW. In vivo MRI cell tracking: clinical studies. AJR Am J Roentgenol 2009; 193(2): 314–325.
183. Brillet PY, Gazeau F, Luciani A, Bessoud B, Cuenod CA, Siauve N, Pons JN, Poupon J, Clement O. Evaluation of tumoral enhancement by superparamagnetic iron oxide particles: comparative studies with ferumoxtran and anionic iron oxide nanoparticles. Eur Radiol 2005; 15(7): 1369–1377.
184. Danhier P, De Preter G, Boutry S, Mahieu I, Leveque P, Magat J, Haufroid V, Sonveaux P, Bouzin C, Feron O, Muller RN, Jordan BF, Gallez B. Electron paramagnetic resonance as a sensitive tool to assess the iron oxide content in cells for MRI cell labeling studies. Contrast Media Mol Imag 2012; 7(3): 302–307.
185. Billotey C, Wilhelm C, Devaud M, Bacri JC, Bittoun J, Gazeau F. Cell internalization of anionic maghemite nanoparticles: quantitative effect on magnetic resonance imaging. Magn Reson Med 2003; 49(4): 646–654.
186. Wilhelm C, Gazeau F, Bacri JC. Magnetophoresis and ferromagnetic resonance of magnetically labeled cells. Eur Biophys J 2002; 31(2): 118–125.
187. Danhier P, De Preter G, Magat J, Godechal Q, Porporato P, Jordan B, Feron O, Sonveaux P, Gallez B. Multimodal cell tracking of a spontaneous metastasis model: comparison between MRI, electron paramagnetic resonance and bioluminescence. Contrast Media Mol Imag 2014; 9(2): 143–153.
188. Terrovitis J, Stuber M, Youssef A, Preece S, Leppo M, Kizana E, Schar M, Gerstenblith G, Weiss RG, Marban E, Abraham MR. Magnetic resonance imaging overestimates ferumoxide-labeled stem cell survival after transplantation in the heart. Circulation 2008; 117(12): 1555–1562.
189. Walczak P, Kedziorek DA, Gilad AA, Barnett BP, Bulte JW. Applicability and limitations of MR tracking of neural stem cells with asymmetric cell division and rapid turnover: the case of the shiverer dysmyelinated mouse brain. Magn Reson Med 2007; 58(2): 261–269.
190. Genove G, DeMarco U, Xu H, Goins WF, Ahrens ET. A new transgene reporter for in vivo magnetic resonance imaging. Nat Med 2005; 11(4): 450–454.
191. Cohen B, Dafni H, Meir G, Harmelin A, Neeman M. Ferritin as an endogenous MRI reporter for noninvasive imaging of gene expression in C6 glioma tumors. Neoplasia 2005; 7(2): 109–117.
192. Vande Velde G, Rangarajan JR, Toelen J, Dresselaers T, Ibrahimi A, Krylychkina O, Vreys R, Van der Linden A, Maes F, Debyser Z, Himmelreich U, Baekelandt V. Evaluation of the specificity and sensitivity of ferritin as an MRI reporter gene in the mouse brain using lentiviral and adeno-associated viral vectors. Gene Ther 2011; 18(6): 594–605.
193. Vande Velde G, Raman Rangarajan J, Vreys R, Guglielmetti C, Dresselaers T, Verhoye M, Van der Linden A, Debyser Z, Baekelandt V, Maes F, Himmelreich U. Quantitative evaluation of MRI-based tracking of ferritin-labeled endogenous neural stem cell progeny in rodent brain. Neuroimage 2012; 62(1): 367–380.
194. Wajnberg E, El-Jaick LJ, Linhares MP, Esquivel DM. Ferromagnetic resonance of horse spleen ferritin: core blocking and surface ordering temperatures. J Magn Reson 2001; 153(1): 69–74.
195. Gilad AA, Winnard PT Jr, van Zijl PC, Bulte JW. Developing MR reporter genes: promises and pitfalls. NMR Biomed 2007; 20(3): 275–290.
196. Paproski RJ, Forbrich AE, Wachowicz K, Hitt MM, Zemp RJ. Tyrosinase as a dual reporter gene for both photoacoustic and magnetic resonance imaging. Biomed Opt Express 2011; 2(4): 771–780.
197. Weissleder R, Simonova M, Bogdanova A, Bredow S, Enochs WS, Bogdanov A, Jr. MR imaging and scintigraphy of gene expression through melanin induction. Radiology 1997; 204(2): 425–429.
198. Fidler IJ. Selection of successive tumour lines for metastasis. Nat New Biol 1973; 242(118): 148–149.
199. Raz A, Hart IR. Murine melanoma: a model for intracranial metastasis. Br J Cancer 1980; 42(2): 331–341.
200. Tatum JL, Kelloff GJ, Gillies RJ, Arbeit JM, Brown JM, Chao KS, Chapman JD, Eckelman WC, Fyles AW, Giaccia AJ, Hill RP, Koch CJ, Krishna MC, Krohn KA, Lewis JS, Mason RP, Melillo G, Padhani AR, Powis G, Rajendran JG, Reba R, Robinson SP, Semenza GL, Swartz HM, Vaupel P, Yang D, Croft B, Hoffman J, Liu G, Stone H, Sullivan D. Hypoxia: importance in tumor biology, noninvasive measurement by imaging, and value of its measurement in the management of cancer therapy. Int J Radiat Biol 2006; 82(10): 699–757.
201. Gallez B, Jordan BF, Baudelet C, Misson PD. Pharmacological modifications of the partial pressure of oxygen in murine tumors: evaluation using in vivo EPR oximetry. Magn Reson Med 1999; 42(4): 627–630.
202. Jordan BF, Gallez B. Surrogate MR markers of response to chemo- or radiotherapy in association with co-treatments: a retrospective analysis of multi-modal studies. Contrast Media Mol Imag 2010; 5(6): 323–332.
203. Danhier P, De Saedeleer CJ, Karroum O, De Preter G, Porporato PE, Jordan BF, Gallez B, Sonveaux P. Optimization of tumor radiotherapy with modulators of cell metabolism: toward clinical applications. Semin Radiat Oncol 2013; 23(4): 262–272.
204. Sonveaux P. Provascular strategy: targeting functional adaptations of mature blood vessels in tumors to selectively influence the tumor vascular reactivity and improve cancer treatment. Radiother Oncol 2008; 86(3): 300–313.
205. Jordan BF, Sonveaux P. Targeting tumor perfusion and oxygenation to improve the outcome of anticancer therapy. Front Pharmacol 2012; 3: 94.
206. Dewhirst MW, Navia IC, Brizel DM, Willett C, Secomb TW. Multiple etiologies of tumor hypoxia require multifaceted solutions. Clin Cancer Res 2007; 13(2 Pt 1): 375–377.
207. Swartz HM, Clarkson RB. The measurement of oxygen in vivo using EPR techniques. Phys Med Biol 1998; 43(7): 1957–1975.
208. Horsman MR, Mortensen LS, Petersen JB, Busk M, Overgaard J. Imaging hypoxia to improve radiotherapy outcome. Nat Rev Clin Oncol 2012; 9(12): 674–687.
209. Ahmad R, Kuppusamy P. Theory, instrumentation, and applications of electron paramagnetic resonance oximetry. Chem Rev 2010; 110(5): 3212–3236.
210. Goda F, O'Hara JA, Rhodes ES, Liu KJ, Dunn JF, Bacic G, Swartz HM. Changes of oxygen tension in experimental tumors after a single dose of X-ray irradiation. Cancer Res 1995; 55(11): 2249–2252.
211. Jordan BF, Misson P, Demeure R, Baudelet C, Beghein N, Gallez B. Changes in tumor oxygenation/perfusion induced by the no donor, isosorbide dinitrate, in comparison with carbogen: monitoring by EPR and MRI. Int J Radiat Oncol Biol Phys 2000; 48(2): 565–570.
212. O'Hara JA, Blumenthal RD, Grinberg OY, Demidenko E, Grinberg S, Wilmot CM, Taylor AM, Goldenberg DM, Swartz HM. Response to radioimmunotherapy correlates with tumor pO2 measured by EPR oximetry in human tumor xenografts. Radiat Res 2001; 155(3): 466–473.
213. Sersa G, Krzic M, Sentjurc M, Ivanusa T, Beravs K, Cemazar M, Auersperg M, Swartz HM. Reduced tumor oxygenation by treatment with vinblastine. Cancer Res 2001; 61(10): 4266–4271.
214. Jordan BF, Gregoire V, Demeure RJ, Sonveaux P, Feron O, O'Hara J, Vanhulle VP, Delzenne N, Gallez B. Insulin increases the sensitivity of tumors to irradiation: involvement of an increase in tumor oxygenation mediated by a nitric oxide-dependent decrease of the tumor cells oxygen consumption. Cancer Res 2002; 62(12): 3555–3561.
215. Sonveaux P, Dessy C, Brouet A, Jordan BF, Gregoire V, Gallez B, Balligand JL, Feron O. Modulation of the tumor vasculature functionality by ionizing radiation accounts for tumor radiosensitization and promotes gene delivery. FASEB J 2002; 16(14): 1979–1981.
216. Jordan BF, Sonveaux P, Feron O, Gregoire V, Beghein N, Gallez B. Nitric oxide-mediated increase in tumor blood flow and oxygenation of tumors implanted in muscles stimulated by electric pulses. Int J Radiat Oncol Biol Phys 2003; 55(4): 1066–1073.
217. Jordan BF, Beghein N, Aubry M, Gregoire V, Gallez B. Potentiation of radiation-induced regrowth delay by isosorbide dinitrate in FSall murine tumors. Int J Cancer 2003; 103(1): 138–141.
218. Jordan BF, Sonveaux P, Feron O, Gregoire V, Beghein N, Dessy C, Gallez B. Nitric oxide as a radiosensitizer: evidence for an intrinsic role in addition to its effect on oxygen delivery and consumption. Int J Cancer 2004; 109(5): 768–773.

219. Sonveaux P, Dessy C, Martinive P, Havaux X, Jordan BF, Gallez B, Gregoire V, Balligand JL, Feron O. Endothelin-1 is a critical mediator of myogenic tone in tumor arterioles: implications for cancer treatment. Cancer Res 2004; 64(9): 3209–3214.
220. Hou H, Khan N, O'Hara JA, Grinberg OY, Dunn JF, Abajian MA, Wilmot CM, Makki M, Demidenko E, Lu S, Steffen RP, Swartz HM. Effect of RSR13, an allosteric hemoglobin modifier, on oxygenation in murine tumors: an in vivo electron paramagnetic resonance oximetry and bold MRI study. Int J Radiat Oncol Biol Phys 2004; 59(3): 834–843.
221. Ansiaux R, Baudelet C, Jordan BF, Beghein N, Sonveaux P, De Wever J, Martinive P, Gregoire V, Feron O, Gallez B. Thalidomide radiosensitizes tumors through early changes in the tumor microenvironment. Clin Cancer Res 2005; 11(2 Pt 1): 743–750.
222. Crokart N, Radermacher K, Jordan BF, Baudelet C, Cron GO, Gregoire V, Beghein N, Bouzin C, Feron O, Gallez B. Tumor radiosensitization by antiinflammatory drugs: evidence for a new mechanism involving the oxygen effect. Cancer Res 2005; 65(17): 7911–7916.
223. Crokart N, Jordan BF, Baudelet C, Ansiaux R, Sonveaux P, Gregoire V, Beghein N, DeWever J, Bouzin C, Feron O, Gallez B. Early reoxygenation in tumors after irradiation: determining factors and consequences for radiotherapy regimens using daily multiple fractions. Int J Radiat Oncol Biol Phys 2005; 63(3): 901–910.
224. Cron GO, Beghein N, Crokart N, Chavee E, Bernard S, Vynckier S, Scalliet P, Gallez B. Changes in the tumor microenvironment during low-dose-rate permanent seed implantation iodine-125 brachytherapy. Int J Radiat Oncol Biol Phys 2005; 63(4): 1245–1251.
225. Ansiaux R, Baudelet C, Jordan BF, Crokart N, Martinive P, DeWever J, Gregoire V, Feron O, Gallez B. Mechanism of reoxygenation after antiangiogenic therapy using SU5416 and its importance for guiding combined antitumor therapy. Cancer Res 2006; 66(19): 9698–9704.
226. Ansiaux R, Baudelet C, Cron GO, Segers J, Dessy C, Martinive P, De Wever J, Verrax J, Wauthier V, Beghein N, Gregoire V, Buc Calderon P, Feron O, Gallez B. Botulinum toxin potentiates cancer radiotherapy and chemotherapy. Clin Cancer Res 2006; 12(4): 1276–1283.
227. Segers J, Di Fazio V, Ansiaux R, Martinive P, Feron O, Wallemacq P, Gallez B. Potentiation of cyclophosphamide chemotherapy using the anti-angiogenic drug thalidomide: importance of optimal scheduling to exploit the 'normalization' window of the tumor vasculature. Cancer Lett 2006; 244(1): 129–135.
228. Crokart N, Jordan BF, Baudelet C, Cron GO, Hotton J, Radermacher K, Gregoire V, Beghein N, Martinive P, Bouzin C, Feron O, Gallez B. Glucocorticoids modulate tumor radiation response through a decrease in tumor oxygen consumption. Clin Cancer Res 2007; 13 (2 Pt 1): 630–635.
229. Hou H, Khan N, Grinberg OY, Yu H, Grinberg SA, Lu S, Demidenko E, Steffen RP, Swartz HM. The effects of Efaproxyn (efaproxiral) on subcutaneous RIF-1 tumor oxygenation and enhancement of radiotherapy-mediated inhibition of tumor growth in mice. Radiat Res 2007; 168(2): 218–225.
230. Jordan BF, Christian N, Crokart N, Gregoire V, Feron O, Gallez B. Thyroid status is a key modulator of tumor oxygenation: implication for radiation therapy. Radiat Res 2007; 168(4): 428–432.
231. Frerart F, Sonveaux P, Rath G, Smoos A, Meqor A, Charlier N, Jordan BF, Saliez J, Noel A, Dessy C, Gallez B, Feron O. The acidic tumor microenvironment promotes the reconversion of nitrite into nitric oxide: towards a new and safe radiosensitizing strategy. Clin Cancer Res 2008; 14(9): 2768–2774.
232. Sonveaux P, Vegran F, Schroeder T, Wergin MC, Verrax J, Rabbani ZN, De Saedeleer CJ, Kennedy KM, Diepart C, Jordan BF, Kelley MJ, Gallez B, Wahl ML, Feron O, Dewhirst MW. Targeting lactate-fueled respiration selectively kills hypoxic tumor cells in mice. J Clin Invest 2008; 118(12): 3930–3942.
233. Mazzone M, Dettori D, Leite de Oliveira R, Loges S, Schmidt T, Jonckx B, Tian YM, Lanahan AA, Pollard P, Ruiz de Almodovar C, De Smet F, Vinckier S, Aragones J, Debackere K, Luttun A, Wyns S, Jordan B, Pisacane A, Gallez B, Lampugnani MG, Dejana E, Simons M, Ratcliffe P, Maxwell P, Carmeliet P. Heterozygous deficiency of PHD2 restores tumor oxygenation and inhibits metastasis via endothelial normalization. Cell 2009; 136(5): 839–851.
234. Ansiaux R, Dewever J, Gregoire V, Feron O, Jordan BF, Gallez B. Decrease in tumor cell oxygen consumption after treatment with vandetanib (ZACTIMA; ZD6474) and its effect on response to radiotherapy. Radiat Res 2009; 172(5): 584–591.
235. Khan N, Mupparaju SP, Hou H, Lariviere JP, Demidenko E, Swartz HM, Eastman A. Radiotherapy in conjunction with 7-hydroxystaurosporine: a multimodal approach with tumor pO2 as a potential marker of therapeutic response. Radiat Res 2009; 172(5): 592–597.
236. Haney CR, Parasca AD, Fan X, Bell RM, Zamora MA, Karczmar GS, Mauceri HJ, Halpern HJ, Weichselbaum RR, Pelizzari CA. Characterization of response to radiation mediated gene therapy by means of multimodality imaging. Magn Reson Med 2009; 62(2): 348–356.
237. Segers J, Crokart N, Danhier P, Gregoire V, Jordan BF, Gallez B. Use of Xanthinol Nicotinate as a co-treatment for radio- and chemotherapy in experimental tumors. Int J Cancer 2010; 126(2): 583–588.
238. Jordan BF, Peeterbroeck J, Karroum O, Diepart C, Magat J, Gregoire V, Gallez B. Captopril and S-nitrosocaptopril as potent radiosensitizers: comparative study and underlying mechanisms. Cancer Lett 2010; 293(2): 213–219.
239. Matsumoto S, Batra S, Saito K, Yasui H, Choudhuri R, Gadisetti C, Subramanian S, Devasahayam N, Munasinghe JP, Mitchell JB, Krishna MC. Antiangiogenic agent sunitinib transiently increases tumor oxygenation and suppresses cycling hypoxia. Cancer Res 2011; 71(20): 6350–6359.
240. Diepart C, Karroum O, Magat J, Feron O, Verrax J, Calderon PB, Gregoire V, Leveque P, Stockis J, Dauguet N, Jordan BF, Gallez B. Arsenic trioxide treatment decreases the oxygen consumption rate of tumor cells and radiosensitizes solid tumors. Cancer Res 2012; 72(2): 482–490.
241. Danhier F, Danhier P, Magotteaux N, De Preter G, Ucakar B, Karroum O, Jordan B, Gallez B, Preat V. Electron paramagnetic resonance highlights that the oxygen effect contributes to the radiosensitizing effect of paclitaxel. PLoS One 2012; 7(7): e40772.
242. Karroum O, Kengen J, Danhier P, Magat J, Mignion L, Bouzin C, Verrax J, Charette N, Starkel P, Calderon PB, Sonveaux P, Feron O, Gregoire V, Gallez B, Jordan BF. Tumor reoxygenation following administration of Mitogen-Activated Protein Kinase inhibitors: a rationale for combination with radiation therapy. Radiother Oncol 2012; 105(1): 64–71.
243. Saito K, Matsumoto S, Yasui H, Devasahayam N, Subramanian S, Munasinghe JP, Patel V, Gutkind JS, Mitchell JB, Krishna MC. Longitudinal imaging studies of tumor microenvironment in mice treated with the mTOR inhibitor rapamycin. PLoS One 2012; 7(11): e49456.
244. Saito K, Matsumoto S, Devasahayam N, Subramanian S, Munasinghe JP, Morris HD, Lizak MJ, Ardenkjaer-Larsen JH, Mitchell JB, Krishna MC. Transient decrease in tumor oxygenation after intravenous administration of pyruvate. Magn Reson Med 2012; 67(3): 801–807.
245. Hou H, Mupparaju SP, Lariviere JP, Hodge S, Gui J, Swartz HM, Khan N. Assessment of the changes in 9 L and C6 glioma pO2 by EPR oximetry as a prognostic indicator of differential response to radiotherapy. Radiat Res 2013; 179(3): 343–351.
246. Swartz HM, Khan N, Buckey J, Comi R, Gould L, Grinberg O, Hartford A, Hopf H, Hou H, Hug E, Iwasaki A, Lesniewski P, Salikhov I, Walczak T. Clinical applications of EPR: overview and perspectives. NMR Biomed 2004; 17(5): 335–351.
247. Matsumoto K, Szajek L, Krishna MC, Cook JA, Seidel J, Grimes K, Carson J, Sowers AL, English S, Green MV, Bacharach SL, Eckelman WC, Mitchell JB. The influence of tumor oxygenation on hypoxia imaging in murine squamous cell carcinoma using [64Cu]Cu-ATSM or [18 F]Fluoromisonidazole positron emission tomography. Int J Oncol 2007; 30(4): 873–881.
248. Mahy P, De Bast M, Gallez B, Gueulette J, Koch CJ, Scalliet P, Gregoire V. In vivo colocalization of 2-nitroimidazole EF5 fluorescence intensity and electron paramagnetic resonance oximetry in mouse tumors. Radiother Oncol 2003; 67(1): 53–61.
249. Tran LB, Bol A, Labar D, Jordan B, Magat J, Mignion L, Gregoire V, Gallez B. Hypoxia imaging with the nitroimidazole 18 F-FAZA PET tracer: a comparison with OxyLite, EPR oximetry and 19 F-MRI relaxometry. Radiother Oncol 2012; 105(1): 29–35.
250. Mason RP, Rodbumrung W, Antich PP. Hexafluorobenzene: a sensitive 19 F NMR indicator of tumor oxygenation. NMR Biomed 1996; 9(3): 125–134.
251. Hunjan S, Mason RP, Constantinescu A, Peschke P, Hahn EW, Antich PP. Regional tumor oximetry: 19 F NMR spectroscopy of hexafluorobenzene. Int J Radiat Oncol Biol Phys 1998; 41(1): 161–171.

252. Yu JX, Kodibagkar VD, Cui W, Mason RP. 19 F: a versatile reporter for non-invasive physiology and pharmacology using magnetic resonance. Curr Med Chem 2005; 12(7): 819–848.
253. Jordan BF, Cron GO, Gallez B. Rapid monitoring of oxygenation by 19 F magnetic resonance imaging: Simultaneous comparison with fluorescence quenching. Magn Reson Med 2009; 61(3): 634–638.
254. Ogawa S, Lee TM, Kay AR, Tank DW. Brain magnetic resonance imaging with contrast dependent on blood oxygenation. Proc Natl Acad Sci U S A 1990; 87(24): 9868–9872.
255. Matsumoto K, Bernardo M, Subramanian S, Choyke P, Mitchell JB, Krishna MC, Lizak MJ. MR assessment of changes of tumor in response to hyperbaric oxygen treatment. Magn Reson Med 2006; 56(2): 240–246.
256. Karczmar GS, River JN, Li J, Vijayakumar S, Goldman Z, Lewis MZ. Effects of hyperoxia on T2* and resonance frequency weighted magnetic resonance images of rodent tumours. NMR Biomed 1994; 7(1–2): 3–11.
257. Robinson SP, Howe FA, Griffiths JR. Noninvasive monitoring of carbogen-induced changes in tumor blood flow and oxygenation by functional magnetic resonance imaging. Int J Radiat Oncol Biol Phys 1995; 33(4): 855–859.
258. Robinson SP, Howe FA, Rodrigues LM, Stubbs M, Griffiths JR. Magnetic resonance imaging techniques for monitoring changes in tumor oxygenation and blood flow. Semin Radiat Oncol 1998; 8(3): 197–207.
259. Howe FA, Robinson SP, McIntyre DJ, Stubbs M, Griffiths JR. Issues in flow and oxygenation dependent contrast (FLOOD) imaging of tumours. NMR Biomed 2001; 14(7–8): 497–506.
260. Baudelet C, Gallez B. How does blood oxygen level-dependent (BOLD) contrast correlate with oxygen partial pressure (pO2) inside tumors? Magn Reson Med 2002; 48(6): 980–986.
261. Baudelet C, Gallez B. Current issues in the utility of Blood Oxygen Level Dependent (BOLD) contrast dependent MR sequences for the assessment of modulations in tumor oxygenation. Current Med Imag Rev 2005; 1: 229–243.
262. Dunn JF, O'Hara JA, Zaim-Wadghiri Y, Lei H, Meyerand ME, Grinberg OY, Hou H, Hoopes PJ, Demidenko E, Swartz HM. Changes in oxygenation of intracranial tumors with carbogen: a BOLD MRI and EPR oximetry study. J Magn Reson Imag 2002; 16(5): 511–521.
263. Elas M, Williams BB, Parasca A, Mailer C, Pelizzari CA, Lewis MA, River JN, Karczmar GS, Barth ED, Halpern HJ. Quantitative tumor oxymetric images from 4D electron paramagnetic resonance imaging (EPRI): methodology and comparison with blood oxygen level-dependent (BOLD) MRI. Magn Reson Med 2003; 49(4): 682–691.
264. Jordan BF, Crokart N, Baudelet C, Cron GO, Ansiaux R, Gallez B. Complex relationship between changes in oxygenation status and changes in R2*: the case of insulin and NS-398, two inhibitors of oxygen consumption. Magn Reson Med 2006; 56(3): 637–643.
265. O'Connor JP, Jackson A, Buonaccorsi GA, Buckley DL, Roberts C, Watson Y, Cheung S, McGrath DM, Naish JH, Rose CJ, Dark PM, Jayson GC, Parker GJ. Organ-specific effects of oxygen and carbogen gas inhalation on tissue longitudinal relaxation times. Magn Reson Med 2007; 58(3): 490–496.
266. McGrath DM, Naish JH, O'Connor JP, Hutchinson CE, Waterton JC, Taylor CJ, Parker GJ. Oxygen-induced changes in longitudinal relaxation times in skeletal muscle. Magn Reson Imag 2008; 26(2): 221–227.
267. O'Connor JP, Naish JH, Parker GJ, Waterton JC, Watson Y, Jayson GC, Buonaccorsi GA, Cheung S, Buckley DL, McGrath DM, West CM, Davidson SE, Roberts C, Mills SJ, Mitchell CL, Hope L, Ton NC, Jackson A. Preliminary study of oxygen-enhanced longitudinal relaxation in MRI: a potential novel biomarker of oxygenation changes in solid tumors. Int J Radiat Oncol Biol Phys 2009; 75(4): 1209–1215.
268. Burrell JS, Walker-Samuel S, Baker LC, Boult JK, Jamin Y, Halliday J, Waterton JC, Robinson SP. Exploring DeltaR(2) * and DeltaR(1) as imaging biomarkers of tumor oxygenation. J Magn Reson Imag 2013; 38(2): 429–434.
269. Jordan BF, Magat J, Colliez F, Ozel E, Fruytier AC, Marchand V, Mignion L, Bouzin C, Cani PD, Vandeputte C, Feron O, Delzenne N, Himmelreich U, Denolin V, Duprez T, Gallez B. Mapping of oxygen by imaging lipids relaxation enhancement: A potential sensitive endogenous MRI contrast to map variations in tissue oxygenation. Magn Reson Med 2013; 70: 732–744.
270. Bacic G, Liu KJ, O'Hara JA, Harris RD, Szybinski K, Goda F, Swartz HM. Oxygen tension in a murine tumor: a combined EPR and MRI study. Magn Reson Med 1993; 30(5): 568–572.
271. Dunn JF, Ding S, O'Hara JA, Liu KJ, Rhodes E, Weaver JB, Swartz HM. The apparent diffusion constant measured by MRI correlates with pO2 in a RIF-1 tumor. Magn Reson Med 1995; 34(4): 515–519.
272. Gallez B, Debuyst R, Liu KJ, Demeure R, Dejehet F, Swartz HM. Development of biocompatible implants of fusinite for in vivo EPR oximetry. MAGMA 1996; 4(1): 71–75.
273. James PE, Bacic G, Grinberg OY, Goda F, Dunn JF, Jackson SK, Swartz HM. Endotoxin-induced changes in intrarenal pO2, measured by in vivo electron paramagnetic resonance oximetry and magnetic resonance imaging. Free Radic Biol Med 1996; 21(1): 25–34.
274. Matsumoto S, Hyodo F, Subramanian S, Devasahayam N, Munasinghe J, Hyodo E, Gadisetti C, Cook JA, Mitchell JB, Krishna MC. Low-field paramagnetic resonance imaging of tumor oxygenation and glycolytic activity in mice. J Clin Invest 2008; 118(5): 1965–1973.
275. Rolett EL, Azzawi A, Liu KJ, Yongbi MN, Swartz HM, Dunn JF. Critical oxygen tension in rat brain: a combined (31)P-NMR and EPR oximetry study. Am J Physiol Regul Integr Comp Physiol 2000; 279(1): R9–R16.
276. Lurie DJ, Bussel DM, Bell BH, Mallard JR. Proton electron double magnetic resonance imaging of free radical solutions. J Magn Reson 1988; 76: 366–370.
277. Lurie DJ, Hutchinson JMS, Bell LH, Nicholson I, Bussel DM, Mallard JR. Field-cycled proton-electron double resonance imaging of free radicals in large aqueous samples. J Magn Reson 1989; 84: 431–437.
278. Grucker D. In vivo detection of injected free radicals by Overhauser effect imaging. Magn Reson Med 1990; 14(1): 140–147.
279. Hyodo F, Murugesan R, Matsumoto K, Hyodo E, Subramanian S, Mitchell JB, Krishna MC. Monitoring redox-sensitive paramagnetic contrast agent by EPRI, OMRI and MRI. J Magn Reson 2008; 190(1): 105–112.
280. Li H, Deng Y, He G, Kuppusamy P, Lurie DJ, Zweier JL. Proton electron double resonance imaging of the in vivo distribution and clearance of a triaryl methyl radical in mice. Magn Reson Med 2002; 48(3): 530–534.
281. Li H, He G, Deng Y, Kuppusamy P, Zweier JL. In vivo proton electron double resonance imaging of the distribution and clearance of nitroxide radicals in mice. Magn Reson Med 2006; 55(3): 669–675.
282. Lurie DJ, Davies GR, Foster MA, Hutchison JM. Field-cycled PEDRI imaging of free radicals with detection at 450 mT. Magn Reson Imag 2005; 23(2): 175–181.
283. Grucker D, Guiberteau T, Eclancher B, Chambron J, Chiarelli R, Rassat A, Subra G, Gallez B. Dynamic nuclear polarization with nitroxides dissolved in biological fluids. J Magn Reson B 1995; 106(2): 101–109.
284. Ardenkjaer-Larsen JH, Laursen I, Leunbach I, Ehnholm G, Wistrand LG, Petersson JS, Golman K. EPR and DNP properties of certain novel single electron contrast agents intended for oximetric imaging. J Magn Reson 1998; 133(1): 1–12.
285. Krishna MC, English S, Yamada K, Yoo J, Murugesan R, Devasahayam N, Cook JA, Golman K, Ardenkjaer-Larsen JH, Subramanian S, Mitchell JB. Overhauser enhanced magnetic resonance imaging for tumor oximetry: coregistration of tumor anatomy and tissue oxygen concentration. Proc Natl Acad Sci U S A 2002; 99(4): 2216–2221.
286. Matsumoto S, Yasui H, Batra S, Kinoshita Y, Bernardo M, Munasinghe JP, Utsumi H, Choudhuri R, Devasahayam N, Subramanian S, Mitchell JB, Krishna MC. Simultaneous imaging of tumor oxygenation and microvascular permeability using Overhauser enhanced MRI. Proc Natl Acad Sci U S A 2009; 106(42): 17898–17903.
287. Kosem N, Naganuma T, Ichikawa K, Phumala Morales N, Yasukawa K, Hyodo F, Yamada K, Utsumi H. Whole-body kinetic image of a redox probe in mice using Overhauser-enhanced MRI. Free Radic Biol Med 2012; 53(2): 328–336.
288. Yamamoto M, Shiba T, Yamada K, Watanabe T, Utsumi H. Noninvasive assessment of the brain redox status after transient middle cerebral artery occlusion using Overhauser-enhanced magnetic resonance imaging J Cereb Blood Flow Metab 2009; 29: 1655–1664.
289. Utsumi H, Yamada K, Ichikawa K, Sakai K, Kinoshita Y, Matsumoto S, Nagai M. Simultaneous molecular imaging of redox reactions monitored by Overhauser-enhanced MRI with 14 N- and 15 N-labeled nitroxyl radicals. Proc Natl Acad Sci U S A 2006; 103(5): 1463–1468.